THE MOLECULAR COMPOSITION OF COMET C/2007 W1 (BOATTINI): EVIDENCE OF A PECULIAR OUTGASSING AND A RICH CHEMISTRY

G. L. Villanueva[1,2], M. J. Mumma[1], M. A. DiSanti[1], B. P. Bonev[1,2], E. L. Gibb[3], K. Magee-Sauer[4], G. A. Blake[5], C. Salyk[6]

ABSTRACT

We measured the chemical composition of comet C/2007 W1 (Boattini) using the long-slit echelle grating spectrograph at Keck-2 (NIRSPEC) on 2008 July 9 and 10. We sampled 11 volatile species (H_2O, OH*, C_2H_6, CH_3OH, H_2CO, CH_4, HCN, C_2H_2, NH_3, NH_2, and CO), and retrieved three important cosmogonic indicators: the ortho-para ratios of H_2O and CH_4, and an upper-limit for the D/H ratio in water. The abundance ratios of almost all trace volatiles (relative to water) are among the highest ever observed in a comet. The comet also revealed a complex outgassing pattern, with some volatiles (the polar species H_2O and CH_3OH) presenting very asymmetric spatial profiles (extended in the anti-sunward hemisphere), while others (e.g., C_2H_6 and HCN) showed particularly symmetric profiles. We present emission profiles measured along the sun-comet line for all observed volatiles, and discuss different production scenarios needed to explain them. We interpret the emission profiles in terms of release from two distinct moieties of ice, the first being clumps of mixed ice and dust released from the nucleus into the sunward hemisphere. The second moiety considered is very small grains of nearly pure polar ice (water and methanol, without dark material or apolar volatiles). Such grains would sublimate only very slowly, and could be swept into the anti-sunward hemisphere by radiation pressure and solar-actuated non-gravitational jet forces, thus providing an extended source in the anti-sunward hemisphere.

Subject headings: comets: general – comets: individual (C/2007 W1 Boattini) – infrared: solar system – astrobiology – astrochemistry.

[1] Solar System Exploration Division, Mailstop 693, NASA Goddard Space Flight Center, Greenbelt, MD, 20771, USA. Geronimo.Villanueva@nasa.gov
[2] Department of Physics, Catholic University of America, Washington, DC 20064.
[3] Department of Physics and Astronomy, University of Missouri, St. Louis, MO 63121
[4] Department of Physics and Astronomy, Rowan University, Glassboro, NJ 08028.
[5] Division of Geological and Planetary Sciences, Caltech, Pasadena, CA 91125.
[6] Department of Astronomy, The University of Texas, 1 University Station, Austin, TX 78712

1. INTRODUCTION

Comets are among the best-preserved bodies in the solar system. Their ices have witnessed a multifaceted formation history in the solar nebula. As comets enter the inner solar system their ices sublimate, releasing into the expanding coma parent volatiles that then are observable at infrared wavelengths through fluorescence. Cometary fluorescence is driven by solar radiation that pumps the molecules into excited vibrational states. They subsequently emit infrared photons through rapid decay to the ground vibrational state in a direct fashion (resonant fluorescence), or through branching into intermediate vibrational levels (non-resonant fluorescence). Collisions are ineffective in exciting these states owing to the low densities and temperatures prevalent in cometary atmospheres. With powerful infrared high-resolution spectrometers these intense fluorescent spectral lines can be measured with high sensitivity, and when combined with new analytical methods we now can characterize the chemical compositions (production rates, isotopic and isomeric ratios, ortho-para ratios, etc.) of comets with unprecedented precision.

Do all these indicators reveal a similar and static formation environment for pre-cometary ices, or do they reflect a more dynamic and continuously evolving formation process? Particularly interesting is whether comets from different dynamical reservoirs (Kuiper Belt, Oort Cloud) shared a common formation path. Recent dynamical models strongly suggest that considerable mixing occurred in the formation region, and thus that comets in a given reservoir originated from diverse regions of the proto-planetary disk. The diversity and fractional representation of sub-populations in each reservoir might differ, making them useful for testing predictions of dynamical models (Mumma & Charnley 2011).

Differences in formation region should be imprinted in the properties of individual comets. Strong compositional diversity of parent volatiles is emerging, but with as yet no unique relationship to dynamical class or inferred reservoir of origin. For instance the two comets showing the most depleted organic chemistry, C/1999 S4 (Mumma et al. 2001) and 73P/SW 3 (Villanueva et al. 2006; DiSanti et al. 2007a; Dello Russo et al. 2007), come from the Kuiper Belt and Oort Cloud reservoirs respectively. At the other extreme, the two comets showing particularly rich organic chemistry, 17P/Holmes (Dello Russo et al. 2008) and C/2001 A2 (Magee-Sauer et al. 2008), come from the Kuiper Belt and Oort Cloud respectively.

These observational discoveries – in concert with new insights obtained through dynamical modeling of transport in the early solar system – indicate a more complex scenario in which both principal comet reservoirs (Kuiper Belt and Oort Cloud) contain bodies formed in diverse regions of the protoplanetary disk (Morbidelli et al. 2005). We emphasize, however, that the fractional representation of each type (enriched, depleted) within a given comet reservoir is as yet poorly constrained, owing to the small number (~ 20) of comets characterized to date at infrared wavelengths. Every additional comet so characterized represents a precious addition to this expanding database and, as the third comet found to be enriched in organic primary volatiles, C/2007 W1 provides an excellent demonstration of this added value.

Comet C/2007 W1 (Boattini) – hereafter Boattini – re-entered the inner solar system for the first time after residing for billions of years in the Oort Cloud (OC), making it dynamically new (Nakano 2008). Discovered by Andrea Boattini through the Mount Lemmon survey in 2007

when it was at (heliocentric distance) 3.3 AU, this comet reached perihelion (0.85 AU) and closest approach to Earth (0.21 AU) in June 2008. This unusually favorable placement produced visual magnitudes around 5 in June-July 2008, making it a very favorable target (Figure 1).

In this paper, we present infrared spectral observations sampling 11 volatile species (H_2O, OH*, C_2H_6, CH_3OH, H_2CO, CH_4, HCN, C_2H_2, NH_3, NH_2, CO) in comet Boattini. We report the molecular parameters derived from them, including rotational temperatures, production rates, abundance ratios, the ortho-para ratios of H_2O and CH_4, and an upper-limit for the D/H ratio in water. We present emission profiles measured along the sun-comet line for all observed volatiles, and discuss different production scenarios necessary to explain these. Lastly, we compare all measured cosmogonic indicators and relate these to a possible formation path for this comet.

2. OBSERVATIONS AND METHODOLOGY

The observations were performed using the long-slit echelle grating spectrograph at Keck-2, NIRSPEC (McLean et al. 1998), on 2008 July 9 and 10. Three instrument settings (KL1, KL2, MWA) were required to sample all species (Table 1). The name of the setting is associated with the adopted instrument configuration (blocking filter, echelle, and cross-disperser grating setttings). The KL1 and KL2 settings sample different portions of the 2.1—4.2 μm spectral region (K and L infrared bands) while the MWA setting samples a portion of the wavelength range 4.4 to 5.5 μm (M infrared band). All settings sample water lines, and therefore abundance ratios (relative to water) are retrieved with high confidence (Mumma et al. 1996; 2003). On July 9, we sampled HDO, CH_3OH, CH_4, C_2H_6 and H_2O with the KL1 setting, and HCN, C_2H_2, NH_3, CH_4, C_2H_6, H_2CO, CH_3OH, NH_2, and H_2O with the KL2 setting; and on July 10, we repeated the

KL1 setting and then sampled the fundamental band of CO (5 lines, v = 1 – 0) along with H_2O (3 lines) in the MWA setting near 4.7 μm.

2a. Data processing

The data were processed using our custom algorithms (tailored for NIRSPEC) to correct for the instrument's anamorphic optics and to calibrate the data in flux and in wavelength (Villanueva et al. 2009; Bonev 2005; DiSanti et al. 2001). The raw frames show strong molecular emissions with very complex spatial distributions. In order to accurately preserve the spatial information of molecular emissions with a precision of one spatial pixel (0.198 arcsec, or 50 km at the comet), exposures were processed individually and were spatially registered using the bright cometary continuum of order 23 (KL1/KL2 settings) and of order 15 (MWA). Inter-order spatial registration was performed using the continuum profiles of the stellar frames (Villanueva et al. 2009; Mandell et al. 2008).

The resulting echellograms (straightened and cropped) reveal emission from parent volatiles with two distinct spatial distributions about the nucleus (symmetric and asymmetric, see echellograms in Figs 2a, 2c, and 3a). This dichotomy distinguishes the outflow properties in Boattini from that of most other comets we observed to date, excepting 103P/Hartley 2 (Mumma et al. 2011). The dissimilar spatial profiles for individual species are especially obvious when they appear in a single spectral order (e.g., C_2H_6 and CH_3OH, Figure 2c).

2b. Rotational temperature

Nucleus-centered spectra were extracted after binning 9 spatial rows along the slit, together spanning ± 0.9 arc-sec (± ~ 230 km) from the nucleus. Examples are shown in Figures 2 and 3.

Rotational temperatures (T_{rot}) were then obtained for three species by correlation and excitation analyses (Bonev 2005; DiSanti et al. 2006; Villanueva et al. 2008). This process requires flux measurements for multiple lines spanning a broad range of excitation energies, along with line-by-line fluorescence models tailored for a range of rotational temperatures (see Table 2). Both conditions were satisfied for H_2O, HCN and C_2H_6 in this comet, and updated fluorescence models were used (§ 2d).

In the excitation analysis for water, we included lines measured in both L-band settings. KL1 samples lines of fairly low rotational excitation that usefully constrain the lower bounds for T_{rot}, while KL2 samples a number of lines of both high and low rotational excitation thereby also constraining the high temperature end of acceptable T_{rot} values. In regions where measurements of individual line fluxes are impeded by severe spectral overlap of emission features of different molecules (most notably, KL2/order25, Fig. 3), we applied a Levenberg–Marquardt non-linear minimization Villanueva et al. 2008 in which all species are fitted simultaneously, permitting robust retrieval of rotational temperature (from HCN) and abundances for all species sampled.

2c. Nuclear Spin Species, spin temperatures, and deuterium abundances

The hydrogen atom carries a nuclear spin angular momentum of $\frac{1}{2}\hbar$. Molecules that contain multiple hydrogen atoms at symmetric positions thus carry a total nuclear spin angular momentum defined by the vector sum of these spins, and that sum is strongly conserved in both radiative and collisional events (Mumma et al. 1987; Bonev et al. 2007; Kawakita et al. 2006). Spin species in cometary water, ammonia (measured through the ortho-para-ratio [OPR] in NH_2), and methane have demonstrated consistent spin temperatures for these species when measured in

a given comet (Mumma & Charnley 2011). However, a statistically significant sample is needed to test whether these measurements may serve as a cosmogonic invariant that traces the origin of these species, and as of today the set of measurements remains very limited.

In the case of water, the molecule is organized in two spin species "ortho" or "para" depending on whether the nuclear spins of its H atoms are parallel or anti-parallel, respectively. The retrieval of the OPR is done simultaneously with the derivation of rotational temperature, since the spectral line intensities depend on both parameters. We applied two methods to retrieve the OPR and T_{rot} in water: a) an iterative process as described in (Bonev et al. 2008), and b) a chi-square minimization technique based on a Levenberg–Marquardt fitting algorithm. The two methods used are complementary and provide practically the same results ([a]: OPR = 2.87 ± 0.15 (1σ), $T_{rot} = 80 \pm 2$ (1σ) K; [b]: OPR = 2.85, T_{rot} = 78 K). We furthermore verified that the final solution is not sensitive to the initially assumed values of both parameters.

Uncertainties derived using the chi-square technique [b], with formal 1-sigma values for the OPR of $\pm$ 0.08 and of $\pm$ 1 for T_{rot}, considerably underestimate the actual error of the retrievals, because these are solely calculated from the stochastic variations of the residual spectrum, and do not integrate systematic errors in the forward model. On the other hand, the iterative process [a], which is based on an excitation analysis, takes also into account the scatter of the line-by-line ratios for transitions with different excitation energy (see F/g diagram in DiSanti et al. 2006 and Bonev et al. 2007, and references therein), and ultimately provides a better quantification of the systematic uncertainties of the retrieved parameters. Specifically, the iterative technique involves retrieving the two parameters independently until the variance around $\langle F / g(T_{rot}(i), OPR) \rangle$ is

minimized. 'F/g(T_{rot}(i), OPR)' is the ratio of the observed line flux to the fluorescence g-factor for an individual line at a specific temperature and OPR, and the weighted mean value ($\langle F/g \rangle$) is averaged over the observed H_2O lines. This iterative process converges to an optimal and unique solution for T_{rot} and OPR. The main sources of systematic error are: 1) assumption of a single temperature for the integrated Field-Of-View (FOV), 2) uncertainties in the branching ratios and cascades that influence the computation of cometary fluorescence efficiencies, and 3) telluric transmittances of the Doppler-broadened cometary transitions.

The retrieval of T_{spin} for methane requires measurements of the abundance ratios among A, E, and F species, which are the three non-combining spin species for a molecule with four identical atoms of spin quantum number ½. The statistical weights of these spin states are 5, 2, and 3, respectively, and in statistical equilibrium the total populations of the individual spin species attain the ratios 5:2:9 (A:E:F). This condition is satisfied for spin temperatures greater than about 60 K. If CH_4 is formed at lower temperatures, the population of a given spin species reflects the energy of the lowest level in that spin ladder, thus increasing the relative population in the 'A' ladder and decreasing those in the 'E' and 'F' ladders; see Fig. 4 in Gibb et al. 2003. Because transitions among spin ladders are strongly forbidden, we treat the A, E, and F transitions as separate molecular species, similar to the ortho and para states of water, to derive the spin temperature of CH_4.

While most transitions of CH_4 in our spectra are unresolved blends of lines from multiple spin species, the R0 line is a pure 'A' transition and the R1 line is a pure 'F' transition. If a common rotational temperature characterizes the populations within the several spin ladders, the 'R0/R1'

intensity ratio is a good diagnostic of the CH_4 spin temperature (Bonev et al. 2009). Although our CH_4 spectra do not permit an independent determination of T_{rot} for methane, we generally find that rotational temperatures determined independently for different molecules on the same date agree within their uncertainties (Table 3). Some gaseous molecules in the coma can cool by emitting radiation in pure rotational transitions, which are permitted for polar species (H_2O, HCN) but not for symmetric species (e.g., CH_4, C_2H_6). Yet the rotational temperature for C_2H_6 agrees well with those of the polar species (Table 3) – demonstrating that collisions (rather than radiative relaxation) control T_{rot} for both polar and apolar species. We expect similar situations for C_2H_6 and CH_4, and thus we adopt T_{rot} = 80 K for the rotational temperature within each CH_4 spin ladder.

Because of the modest Doppler shift of Boattini (+13 km s^{-1}) most methane lines are strongly affected by atmospheric absorption. R0, R1, R2, and P2 are the least affected, so we decided to include the measurements of P2 and R2 doublets in our analysis to further constrain the spin temperature. Considering these four lines we obtain an optimum excitation analysis at 'F/A' = 1.57 ± 0.48 (1σ) and 'E/A' < 11.31 (3σ), but taking into consideration the asymptotic relationship between A/E/F and T_{spin}, our measurements cannot distinguish spin relaxation from equilibrium, leading to the meaningful lower limit of $T_{spin}(CH_4) > 19$ K.

When searching for deuterated water, the modest water production rate of comet Boattini (1.2×10^{28} s^{-1}, Table 3) limited the sensitivity of our measurement of D/H in water. Considering data taken on both nights (July 9 and July 10 UT) with a total of 40 minutes of integration, we

obtained an upper limit (3σ) of D/H < 12.9 x 10^{-4} (8.3 VSMOW); see Villanueva et al. 2009 for comparison with other comets.

2d. Nucleus-centered Production rates

We extracted calibrated fluxes for multiple ro-vibrational lines of each molecule from spectra centered on the nucleus (the 9-row extracts). Rotational temperatures in the sampled area (0.432 x 1.800 arc-sec^2 ~ 110 x 460 km^2) were retrieved for H_2O, HCN, and C_2H_6 using updated fluorescence efficiencies (g-factors) that include fluorescence cascades for H_2O and HCN (see below). Nucleus-centered production rates (Q_{nc}) were then obtained from the fluxes and rotational temperatures, using an outflow velocity of $v_0 = 800\ R_h^{-0.5}$ m s^{-1}. Our fluorescence efficiencies (g-factors) are based on updated quantum-mechanical models for C_2H_6 (Villanueva et al. 2011a), H_2O, HDO, HCN, CH_4, CH_3OH, CO, C_2H_2 (Villanueva et al., in prep.) H_2CO (DiSanti et al. 2006), NH_2 , and NH_3 (Villanueva et al., in prep.; see also Kawakita & Mumma 2011).

The new C_2H_6 model includes a proper treatment of the branching ratios of the -split levels of ν_7 vibrational level, a set of updated molecular constants and the inclusion of P- and R-branches totaling 17,266 spectral lines. Results achieved with the new model are compared with those from the previous model (Dello Russo et al. 2001) in Figure 4a. The new H_2O model makes use of the latest spectral databases (BT2: Barber et al. 2006, GEISA: Jacquinet-Husson et al. 2009, HITRAN: Rothman et al. 2009 and HITEMP: Rothman et al. 2010) to compute full non-resonance fluorescence for 500 million transitions (Villanueva et al. 2011d). Results achieved with the new model are compared with those from the previous model (Dello Russo et al. 2005)

in Figure 4c. The HCN model considers updated molecular constants and cascade from upper levels based on the extensive spectral database of Harris et al. 2006. For the case of NH_3, we consider spectral constants from 3 line atlases (TROVE: Yurchenko et al. 2009; 2011, GEISA and HITRAN), allowing us to compute line-by-line and level-by-level branching ratios with high precision. We adopt the model of Kawakita & Mumma 2011 for NH_2, but choose to use our g-factors for NH_3 since our model accounts for all possible hot and cold bands. This leads to a slight decrease in the g-factors for the three NH_3 lines detected (see comparison in Table 2) and thus to a corresponding increase in the retrieved production rate. All new fluorescence models consider a highly realistic solar pumping flux, which is a combination of a theoretical continuum model and a highly precise solar line list, instead of the normally assumed black-body model; cf., Appendix C of Villanueva et al. 2011a.

As presented in Figure 4, the new models provide improved fits to fluorescence intensities for C_2H_6, HCN, and H_2O in Boattini, although differences in the line-by-line ratios for 'Q' still exceed the level expected from stochastic noise alone. Sources of systematic uncertainty include: a) the computation of telluric transmittances for Doppler-broadened cometary lines requires precision in the spectral atlas that is not yet available; b) the description of perturbations (Fermi, Coriolis) for individual line intensities in ab-initio models require experimental parameters that are not always available; and c) instrumental artifacts (such as row-chop in the acquisition electronics) that cannot be fully compensated. Further laboratory studies will be needed to properly assess the accuracy of currently available hot-band intensities predicted from ab-initio models, in particular for infrared g-factors with significant cascade contributions (e.g. H_2O and NH_3).

2e. Spatial Profiles & Growth factors

In order to derive global production rates from nucleus-centered values (previous section), we determined the slit-losses from analyses of the spatial profiles (see Fig. 5) of select volatile species measured individually along the slit (the so-called "Q-curve methodology"); see Fig. 6c. Earth's atmospheric turbulence introduces a blurring and shifting of the spatial profiles, an effect normally termed "atmospheric seeing". As shown in Fig. 6a/b, atmospheric seeing causes the image of a point source to spread both along and across the slit dimensions, and thus the measured flux from the comet is less sharply peaked about the nucleus than it would be in the absence of this seeing, causing the measured intensity to be less than the value expected if 'seeing' were absent – an effect usually termed 'slit losses'.

In the Q-curve analysis, we properly correct for slit losses by multiplying Q_{nc} by a growth factor "GF" ($GF = Q_{term}/Q_{nc} = \langle Q_2, Q_3, Q_4, Q_5 \rangle / \langle Q_0, Q_1 \rangle$, where $\langle\rangle$ denotes a weighted mean operation. We compute production rates at intervals stepped along the slit (Q2 through Q5) (Fig. 6c), invoking uniform symmetric outflow at each position along the slit. We then symmetrize the production rates by taking the mean of up- and down-slit measurements ($\langle Q_2 \rangle = 0.5(Q_{2+} + Q_{2-})$. The mean of Q's taken at symmetric positions about the center corrects for axisymmetric outflow, and its increase from the nucleus-centered position to a terminal value establishes the 'growth factor', see Xie & Mumma 1996; Dello Russo et al. 1998. This correction is valid for both symmetric and asymmetric outflow about the nucleus, if release occurs only at the nucleus and the outflow velocity is independent of azimuth about the nucleus (Xie & Mumma 1996). However, the outflow of material in comet Boattini is somewhat more complex, introducing the possible presence of extended release for some species.

Gases in comet Boattini revealed two distinct and very different spatial profiles about the nucleus (Fig. 5a/b/c). The polar molecules H_2O and CH_3OH show very asymmetric profiles with an extended profile in the anti-sunward hemisphere, while C_2H_6 and HCN show particularly symmetric profiles. Results for CH_4 and CO are also indicative of symmetric profiles, but the Doppler shift of the comet (+13 km s^{-1}) restricted a sensitive measurement of the spatial profiles for these species. We discuss the measured profiles in terms of two outgassing sources: I: symmetric release, II: asymmetric release). The presence of both nuclear and extended sources would complicate the evaluation of growth factors (Fig. 6c).

For molecules with symmetric profiles (C_2H_6, HCN), we measured a GF_{sym} of 1.63 from the night and day spatial profiles (Fig. 6c), and we scaled the nucleus-centered Q's by this factor to correct for slit losses and seeing effects ($Q_{gas} = GF_{sym} \times Q_{nc}$). The spatial profiles of the hypervolatiles (CH_4 and CO) show a higher correlation with the symmetric profile (88%) than with the asymmetric profile (75%), and therefore we estimate that these species are better described with a symmetric outgassing source. In the case of H_2O and CH_3OH (asymmetric spatial profiles, Fig. 5a), we assumed that the observed profiles are related to two sources, and herewith the spectral extract contains emission originating from a "nuclear" or isotropic source (I) and an "extended" or asymmetric source (II). Production rates and mixing ratios (Table 3) are given for type I sources only, since they are better described with an isotropic outgassing model. The uncertainties given there reflect the level of agreement among production rates obtained independently from different lines of the same species. We verified that the reported values are (at worst) only weakly influenced by uncertainties in the rotational temperature. Column

densities for source II (taken at successive positions along the slit) reveal an intensity maximum at a distance of ~400 km from the nucleus, and a monotonic increase in the II/(I+II) ratio at greater distances from the nucleus (Table 4).

3. DISCUSSION

Comet Boattini was only a moderately active comet, with a figure of merit of 0.36 [FM = $Q(H_2O) \times 10^{-29} R_h^{-1.5} \Delta^{-1}$, Mumma et al. 2003] based on our measured production rate (Table 3).. However, owing to the unusually large mixing ratios of trace volatiles we obtained a comprehensive view of the comet's composition with total integration time per setting of only 20 minutes. The high sensitivity and broad spectral grasp provided by NIRSPEC at Keck II allowed us to simultaneously detect numerous lines of eight volatiles (including H_2O, Table 2) and to obtain their spatial distributions.

3.1 Coma asymmetries

Boattini is the first comet that clearly displayed distinct spatial distributions about the nucleus for individual parent volatiles, and 103P/Hartley 2 was the second (Mumma et al. 2011). In Boattini, the polar molecules H_2O and CH_3OH show very asymmetric profiles with an extended profile in the anti-sunward hemisphere, whereas C_2H_6, HCN and presumably CH_4 and CO show symmetric profiles about the nucleus and along the sun-comet line (§ 2e).

Primary volatiles in Hartley-2 showed the opposite behavior near the nucleus, with H_2O and CH_3OH being nearly symmetric while C_2H_6 showed strong asymmetry about the nucleus and HCN was intermediate. Images from the Deep Impact spacecraft on the EPOXI mission showed

that the comet was shedding large clumps of water ice that achieved only very slow radial velocity (< 2 m s^{-1}, A'Hearn et al. 2011) and vaporized within 30 km of the nucleus. Therefore, the H_2O sublimated from them would bear the signature of thermal gas velocities (~400 m s^{-1}) rather than the bulk outflow velocity of gas released from the nucleus (Mumma et al. 2011). Because such clumps would likely be rapid rotators, the spatial distribution of water released from them would be isotropic, in contrast with the asymmetric spatial profiles of volatiles released directly from the nucleus. Interestingly, some chunks of large icy grains did survive longer and were accelerated by non-gravitational forces in the anti-sunward direction far from the nucleus (>10,000 km), as revealed from the water excess detected with Herschel in the tail direction (Meech et al. 2011).

If in Boattini all volatile species were released by subliming directly from the nucleus, the spatial profiles would be extended in the sunward hemisphere for all species – this is not seen. If instead, water and other species were released as clumps of mixed ices carried outward from the nucleus at very slow velocity, their sublimation would produce symmetric distributions for both apolar species and water (as in Hartley-2), and the spatial profiles of all components would be similar to those of Figure 5b – this is also not seen. A hybrid release (Sources I & II) could work, if clumps of a mixed ice (polar and apolar species, Source I) were released along with tiny grains of nearly pure polar ice (Source II). The profiles for Source I (H_2O, CH_3OH, C_2H_6, HCN, etc.) would then be represented by those of Fig. 5b (C_2H_6, HCN, etc.).

An extended source of water vapor in the anti-sunward hemisphere might arise if very small grains of nearly pure polar ice (Source II, water and methanol, without dark material or apolar

volatiles) are released in large quantities. Lacking absorptive dust, they would warm (and sublime) at a much slower pace. Radiation pressure and solar-actuated non-gravitational jet forces (assuming anisotropic gas release in the sunward direction from the grain) might accelerate them to high terminal velocity, pushing them into the anti-sunward hemisphere where they would continue to slowly vaporize. They could also become electrically charged – negatively by electron attachment or positively by the photoelectric effect – permitting magnetic pickup by the solar wind beyond the contact surface (outer boundary of the diamagnetic cavity) and well beyond our FOV. Like gaseous ions in the tail, such charged grains could be accelerated to large terminal velocities and transported into the anti-sunward hemisphere before vaporizing (Horanyi & Mendis 1985). In either case, the water cloud so produced would continue to move down-sun at the terminal (center of mass) velocity, while also expanding radially, and thus it could produce the asymmetric properties inferred for Source II. Further discussion is deferred to a future publication.

The continuum emission of comet Boattini follows the spatial profile of H_2O and CH_3OH, demonstrating that it is associated with both Sources (I and II). The continuum intensity is notably enhanced at wavelengths in the spectral range 3.2-3.6 μm (3100 -2800 cm^{-1}), where many organics have strong emissions (see Fig. 7). This excess could be due to "organic refractory grains", "methanol-water ice grains", or perhaps to several weak bands of ethane and methanol (plus other aliphatic and aromatic volatiles with bands in this spectral region). Silicate grains cannot produce this spectral signature.

Several independent studies provide support for the scenario outlined above. In comet C/2000 WM_1, Tozzi et al. 2004 observed two solid sublimating components with different lifetimes. They concluded that the secondary source was probably related to certain organic grains and not to water ice mantled grains (with dark cores) since these have much shorter lifetimes than the long lifetimes needed to explain their data. The moieties described above for Boattini could provide two sources with different lifetimes, as required by Tozzi et al. In comet 9P/Tempel 1, Sunshine et al. 2006 detected a cloud of pure water ice grains in the ejecta excavated by the Deep Impact (DI) event (A'Hearn et al. 2005), perhaps an analogue to the small polar ice grains that we observe in the anti-sunward coma of comet Boattini. Consistent with this view, Mumma et al. 2005 and DiSanti et al. 2007b associated the "delayed" release of certain volatiles in the ejecta cloud with the deferred sublimation of fast moving small icy grains.

If we assume that at 500 km source II is fully developed, we estimate the strength of source II to be at least ~3 times stronger than Source I in the anti-sunward hemisphere (see Table 4). Considering that this source is only hemispheric, the equivalent isotropic production rate would be 1.5 for source II, and therefore the actual global water production (sources I and II) is at least 2.5 higher than what we measure for source I only.

3.2 Organic composition

Comet Boattini appears to be highly enriched in volatiles relative to water (Table 3, Fig. 8), with very high values for HCN (0.50 ± 0.01), NH_3 (1.74 ± 0.17), C_2H_6 (1.96 ± 0.04) and CH_3OH (3.78 ± 0.12); values are in percent and uncertainties are 1-sigma. We usually tend to associate enrichment in organics with formation in cold regions followed by limited thermal processing

prior to their final incorporation into the nucleus. This is particularly the case for hypervolatiles (CO and CH_4), which are preferentially lost through vaporization in warmer nebular environments and whose cometary abundance is used to test thermal processing. However, this apparent enrichment may originate because not all the water is in the vapor phase (the phase we sample), and additional sources may be releasing water vapor into the coma in a delayed fashion (source II). The extended spatial profile observed for gaseous water may be indicative of additional release from icy grains carried beyond the nucleus (see further discussion in § 3.2).

If we assume a production rate of polar species to be 2.5 times higher than that indicated for source I alone (see section 3.1), the comet appears mostly depleted in organics, instead of enriched (see Fig. 8). Consequently, relative abundance ratios among the trace species might be better diagnostics of the nuclear ice composition. Again, we caution that the standard model we use (for relating the spatial distribution of a primary volatile to its production rate) is not well tailored for interpreting the production from tiny "polar ice grains". The fraction of total water (and other volatiles) contained in source II is poorly constrained, owing to uncertainties in the extended source properties (e.g., outflow velocity, acceleration, grain lifetime, etc.). Figure 8 should be taken as illustrative only.

The C_2H_6/C_2H_2 and CH_3OH/CO ratios are thought to be controlled by H-atom addition reactions on the surfaces of interstellar grains prior to their incorporation into the nucleus. These reactions are strongly dependent on the X-ray flux and temperature to which the pre-cometary grains were exposed (and to the H-atom densities), and thus these abundance ratios behave as sensitive "thermometers" of the conditions to which pre-cometary grains were exposed. Watanabe et al.

2004 found maximum conversion efficiencies at low temperatures (10-20 K), for which H-atom retention is favorable. In late stages, increased nebular clearing permits X-ray penetration to larger heliocentric distances. This triggers increased H-atom densities, through photoionization of nebular H_2 followed by H-atom production via recombination reactions.

The hydrogenation reaction chain for methanol starts with hydrogen-atom addition to CO producing the highly reactive formyl radical (HCO), which subsequently converts to monomeric formaldehyde (H_2CO), which is ultimately converted to CH_3OH (Hudson & Moore 1999), formic acid (H_2CO_2) or other formaldehyde polymers (e.g., polyoxymethylene, POM). Likewise, C_2H_6 can be produced by hydrogen addition from acetylene (C_2H_2) ice with C_2H_4 as an intermediate species in the conversion chain (Hiraoka et al. 2000).

Measuring the efficiency of this process in pre-cometary material from the abundance ratio of CH_3OH/CO in cometary atmospheres becomes convoluted due to the large differences in volatility among these species, and the possible radial mixing of material in the protoplanetary disk. Other products (e.g., H_2CO) are perhaps more suitable to test this type of processing. Comet Boattini is among the comets with highest CH_3OH/H_2CO and C_2H_6/C_2H_2 ratios from our sample of comets at infrared wavelengths, in contrast to comets like C/1999 S4 and 73P/Schwassmann-Wachmann whose chemistry suggests extremely low conversion efficiency (Mumma et al. 2001; Villanueva et al. 2006; Dello Russo et al. 2007). As discussed by Villanueva et al. 2006, different formation regions or times when the ices were accreted may explain the observed differences in hydrogenation among comets. Considering the high C_2H_6/C_2H_2 and CH_3OH/H_2CO and high spin temperatures (see section §3.3), we infer that the

comet may have formed in the outer regions of the planetary system after the partial clearing of the nebula. The fact that the spin temperature of water indicates a value at which hydrogenation efficiency is expected to be relatively low is on the other hand puzzling. As more measurements are obtained for these indicators in comets (and in the lab), a better understanding of their relationship to cosmogonic conditions will be revealed.

3.3 Ortho-para ratios, deuterated species and formation temperature

The abundance ratios amongst isotopologues and spin isomers are thought to be excellent diagnostics of the formation path of cometary ices, since these ratios are sensitive to formation and/or subsequent processing prior to incorporation into the cometary nucleus. At infrared wavelengths, multiple cometary lines of spin-isomeric (ortho, para) and isotopic forms (H_2O, HDO) of water and methane (CH_4: A/E/F, CH_3D) are observable in the 2.8-3.8 μm spectral region, allowing us to retrieve information about the environment where these ices were formed.

For comet Boattini, the measured cosmogonic parameters indicate formation temperatures higher than 14K (D/H), higher than 19K ($T_{spin}[CH_4]$) and higher than 34K ($T_{spin}[H_2O]$), all being self-consistent, and with water OPR providing the most stringent constraint on the lower-bound for the formation temperature (see Table 5).

In particular, the D/H ratio is notably sensitive to the range of temperatures where comets were formed (T<80K), and can be used to assess a representative formation temperature Millar et al. 1989 considering gas-phase chemistry only. This pioneering work has since been extended to full models of protoplanetary disks, which include a realistic treatment of turbulent viscosity and

condensation (Drouart et al. 1999; Mousis et al. 2000), permitting us to relate the D/H ratio not only to a formation temperature but to a location in the solar nebula. New models also include complex hydrodynamic schemes with realistic radiative transfer processes (Willacy & Woods 2009) that (when combined with a broad chemical network) allow us to better interpret the primordial conditions of the formative region. The HDO/H_2O upper limit (< 0.0026) is highly significant in comparison with the Willacy & Woods 2009 model, that predicts about an order of magnitude higher ratios in the protoplanetary disk mid-plane. Two possible reasons for this discrepancy between our upper limit and their predicted value are 1) they assumed a temperature of 10 K in the proto-solar cloud core from which the disk was formed – such low temperatures heavily favor a high degree of deuteration; and 2) the lack of radial mixing in the modeled disks, which can diminish D/H in comet-forming environments via outward transport of less fractionated water from the inner solar system.

4. CONCLUSIONS

We report quantitative measures of the chemical composition and outgassing morphology of comet C/2007 W1 (Boattini). We measured production rates for 10 volatile species (H_2O, OH*, C_2H_6, CH_3OH, H_2CO, CH_4, HCN, C_2H_2, NH_3, CO), and retrieved three important cosmogonic indicators: the ortho-para ratios of H_2O and CH_4, and an upper-limit of the D/H ratio in water. The abundances of almost all volatiles (relative to water) are among the highest ever observed in a comet, with very high values for CH_3OH, HCN, NH_3 and C_2H_6 (see Table 3). In particular the comet's chemical composition indicates efficient hydrogenation of the pre-cometary grains, with C_2H_6/C_2H_2 and CH_3OH/H_2CO ratios among the highest ever observed.

If the measured spin temperatures of CH_4 and H_2O indicate formation temperatures, the pre-cometary ices in comet Boattini formed in outer parts of the solar system. The high C_2H_6/C_2H_2 and CH_3OH/H_2CO abundance ratios suggest this formation occurred after partial clearing of the nebula, when hydrogenation can be enhanced by penetration of X-rays into the formative region.

The singular nature of the comet's chemical taxonomy is also accompanied by a peculiar icy grain structure as revealed by its complex outgassing pattern, indicative perhaps of two-moieties of ice that sublimate with different lifetimes. The conventional view is that water sublimation controls the release of parent volatiles in comets, and thus that spatial profiles of most parent volatiles should be related. Our results suggest a more complex release process in Boattini –in which two forms of release are present. In the first, clumps of mixed ice and dust are released from the nucleus into the sunward hemisphere, perhaps by the release of abundant CO_2 as in Hartley-2. Their sublimation could produce spherically symmetric gas and dust distributions similar to those seen by Mumma et al. 2011 for water, methanol, ethane, and dust in Hartley-2.

In the second moiety, very small grains of nearly pure polar ice (water and methanol, without dark material or apolar volatiles) may be released in large quantities. Lacking absorptive dust, they would warm (and sublime) at a much slower pace. If affected by radiation pressure and solar-actuated non-gravitational jet forces, they would accelerate to large terminal velocities and be transported into the anti-sunward hemisphere before vaporizing. In this way, they could produce an asymmetric excess of the polar H_2O and CH_3OH species in the anti-sunward direction. The congruence of the spatial profiles for continuum with polar volatiles (H_2O and CH_3OH) may also suggest the presence of a population of naked rocky grains released along

with the grains of nearly pure polar ice. The combination could be the signature of earlier re-processing of primordial ices within the near-surface layer of the cometary nucleus.

Further studies will be required to better understand such a fascinating body, and insights gained from data taken pre and post-perihelion with CRIRES at VLT (DiSanti et al., in prep.) may assist in this regard.

ACKNOWLEDGEMENTS

GLV, MJM, MAD and BPB acknowledge support from NASA's Astrobiology Institute (RTOP 344-53-51), and NASA's Planetary Atmospheres and Astronomy Programs (RTOPs 344-32-07, 08-PAST08-0034, 08-PATM08-0031). BPB and ELG acknowledge support from the NSF Astronomy and Astrophysics Grants Program (AST-0807939), and KMS from the NSF RUI Program. GAB acknowledges support from the NASA Origins of Solar Systems program. We thank James Lyke and the staff of Keck Observatory for general support. The data presented herein were obtained at the W. M. Keck Observatory operated as a scientific partnership among CalTech, UCLA, and NASA. This Observatory was made possible by the generous financial support of the W. M. Keck Foundation. The authors wish to recognize and acknowledge the very significant cultural role and reverence that the summit of Mauna Kea has always had within the indigenous Hawaiian community. We are most fortunate to have the opportunity to conduct observations from this mountain.

TABLE 1. OBSERVING LOG

Date [UT]	Time [UT]	Setting	Molecules sampled	R_h [AU]	v_h [km s^{-1}]	Δ [AU]	Δ-dot [km s^{-1}]	AM	Slit PA [deg]	Comet PA [deg]
July 9 2008	14:18 14:47	KL1	H_2O, CH_3OH, C_2H_6, CH_4	0.893	9.77	0.348	12.91	1.97	241-248	248
	14:54 15:32	KL2	H_2O, H_2CO, CH_4, HCN, C_2H_2, NH_3	0.893	9.79	0.348	12.96	1.52	250-261	248
July 10 2008	14:18 14:31	MWA	H_2O, CO	0.898	10.34	0.356	12.92	1.94	242-246	248
	14:42 15:27	KL1	H_2O, CH_3OH, C_2H_6, CH_4	0.899	10.36	0.356	12.98	1.51	248-261	248

The ephemeris values are given for the midpoint of the time interval, where R_h is the heliocentric distance of the comet, v_h is the heliocentric velocity of the comet, Δ is the geocentric distance, Δ–dot is the topocentric velocity, PA indicates "position angle" and AM indicates "airmass".

1
2 TABLE 2. OBSERVED EMISSION LINES AND RELEVANT PARAMETERS

Transition	Frequency [cm^{-1}]	Flux 10^{-20} [W m^{-2}]	± Flux (1σ) 10^{-20} [W m^{-2}]	g-factor [s^{-1}]*	E_{rot} [cm^{-1}]	Atmospheric transmittance
July/9/2008 – H_2O ortho at 80K – gfactors x 10^{-9}						
$(101)0_{00}$-$(001)1_{11}$	3458.12	19.76	1.03	73.63	35.77	0.73
$(101)4_{22}$-$(100)5_{23}$	3456.45	9.62	1.28	90.67	438.87	0.30
$(003)4_{22}$-$(002)5_{23}$	3453.45	51.28	1.58	0.30	433.07	0.89
$(210)1_{01}$-$(011)0_{00}$	3453.39			0.35	0.00	0.90
$(200)1_{10}$-$(100)2_{21}$	3453.30			79.33	131.64	0.67
$(101)2_{02}$-$(100)3_{21}$	3453.15			70.49	207.71	0.90
$(200)1_{10}$-$(001)1_{11}$	3450.29	38.92	1.17	110.23	35.77	0.73
$(101)5_{24}$-$(100)6_{25}$	3449.38	7.75	1.11	23.56	542.34	0.80
$(300)2_{12}$-$(200)1_{01}$	3449.30			0.58	23.04	0.79
$(201)4_{13}$-$(101)3_{22}$	3428.46	13.02	1.50	0.17	195.76	0.79
$(200)2_{12}$-$(001)2_{11}$	3428.30			50.91	93.46	0.56
$(101)5_{42}$-$(001)6_{33}$	3417.79	12.05	1.10	0.12	652.10	0.93
$(101)3_{22}$-$(001)4_{13}$	3417.78			6.33	271.88	0.93
$(200)3_{12}$-$(100)4_{23}$	3417.66			22.47	294.26	0.93
$(200)7_{07}$-$(100)7_{16}$	3417.56			0.04	691.36	0.93
$(001)6_{06}$-$(000)7_{25}$	3413.07	25.11	1.63	2.99	782.41	0.58
$(200)2_{12}$-$(100)3_{21}$	3412.92			62.77	207.71	0.85
$(300)3_{03}$-$(101)2_{02}$	3411.70	24.92	1.06	0.40	68.10	0.98
$(101)3_{13}$-$(001)4_{04}$	3411.62			52.24	218.70	0.98
$(201)0_{00}$-$(200)1_{01}$	3388.77	16.37	1.42	29.79	23.04	0.95
$(101)7_{35}$-$(100)8_{36}$	3388.65			0.06	986.95	0.97
$(101)4_{31}$-$(001)4_{40}$	3388.58			0.08	468.92	0.97
$(101)4_{04}$-$(001)5_{15}$	3387.54	9.50	1.28	25.93	320.97	0.88
$(201)2_{11}$-$(101)2_{02}$	3385.17	9.49	2.01	1.00	68.10	0.71
$(101)2_{11}$-$(001)3_{22}$	3385.14			23.82	200.74	0.71
$(200)6_{25}$-$(100)7_{16}$	3384.89			0.19	691.36	0.56
$(200)2_{12}$-$(001)3_{13}$	3382.10	69.25	1.47	164.44	139.66	0.95
$(200)3_{21}$-$(100)4_{32}$	3374.40	7.79	1.48	16.94	373.79	0.92
$(200)2_{21}$-$(001)3_{22}$	3372.75	35.43	1.39	90.11	200.74	0.96
$(300)1_{01}$-$(101)0_{00}$	3372.60			0.91	0.00	0.95
$(201)1_{11}$-$(200)2_{12}$	3369.73	9.79	1.77	23.93	76.15	0.89
$(200)3_{03}$-$(001)4_{04}$	3358.92	25.18	1.56	80.49	218.70	0.78
July/9/2008 – H_2O para at 80K – gfactors x 10^{-9}						
$(200)2_{20}$-$(001)2_{21}$	3445.89	11.39	1.27	34.65	129.81	0.67
$(120)2_{20}$-$(020)3_{31}$	3435.57	6.41	0.97	0.29	348.88	0.82
$(200)3_{22}$-$(001)3_{21}$	3435.49			11.81	206.99	0.95
$(101)2_{12}$-$(001)3_{03}$	3434.40	16.82	1.29	21.87	134.90	0.95

$(101)4_{14}$-$(100)4_{31}$	3434.38			1.34	374.80	0.94
$(200)2_{11}$-$(100)3_{22}$	3434.33			18.53	201.82	0.92
$(101)4_{32}$-$(001)5_{23}$	3415.84	8.74	1.18	0.15	440.04	0.92
$(201)1_{10}$-$(200)1_{11}$	3415.80			7.44	35.27	0.86
$(101)3_{03}$-$(100)4_{22}$	3415.73			16.80	309.51	0.86
$(101)4_{14}$-$(001)5_{05}$	3390.09	10.06	1.40	7.87	320.21	0.92
$(101)2_{12}$-$(100)3_{31}$	3390.02			21.68	278.16	0.86
$(200)2_{02}$-$(001)3_{03}$	3378.48	22.69	1.69	46.57	134.90	0.93
$(200)2_{11}$-$(001)3_{12}$	3366.35	9.03	1.90	34.41	170.93	0.49
$(200)3_{13}$-$(001)4_{14}$	3360.99	9.67	1.46	27.10	221.33	0.85
$(201)2_{12}$-$(200)3_{13}$	3349.38	4.32	1.36	8.98	136.71	0.97
July/10/2008 – H_2O ortho at 79K – gfactors x 10^{-9}						
$(201)0_{00}$-$(200)1_{01}$	3388.77	13.44	0.97	30.17	23.04	0.96
$(101)7_{35}$-$(100)8_{36}$	3388.65			0.06	986.95	0.97
$(200)2_{12}$-$(001)3_{13}$	3382.10	67.98	1.31	165.61	139.66	0.96
$(200)3_{21}$-$(100)4_{32}$	3374.40	6.41	1.07	16.57	373.79	0.94
$(200)2_{21}$-$(001)3_{22}$	3372.75	39.35	1.11	90.72	200.74	0.97
$(300)1_{01}$-$(101)0_{00}$	3372.60			0.92	0.00	0.96
$(201)1_{11}$-$(200)2_{12}$	3369.73	10.84	1.31	24.07	76.15	0.91
$(210)2_{21}$-$(110)3_{30}$	3361.03	2.97	1.07	8.46	303.83	0.88
$(200)3_{03}$-$(001)4_{04}$	3358.92	27.06	1.15	80.01	218.70	0.80
$(001)1_{11}$-$(010)1_{10}$	2151.20	173.20	18.96	451.12	45.75	0.89
$(100)2_{21}$-$(010)1_{10}$	2148.19	38.42	17.43	117.99	45.75	0.95
$(001)2_{20}$-$(010)2_{21}$	2144.81	73.64	18.30	200.34	147.56	0.93
$(001)0_{00}$-$(010)1_{01}$	2137.38	27.66	29.27	530.28	23.81	0.56
$(001)3_{22}$-$(010)3_{21}$	2137.33			47.78	224.59	0.24
July/10/2008 – H_2O para at 79K – gfactors x 10^{-9}						
$(101)4_{14}$-$(001)5_{05}$	3390.09	8.55	0.95	7.75	320.21	0.94
$(101)2_{12}$-$(100)3_{31}$	3390.02			21.78	278.16	0.88
$(200)2_{02}$-$(001)3_{03}$	3378.48	23.57	1.35	46.58	134.90	0.94
$(200)3_{13}$-$(100)4_{22}$	3371.69	4.32	0.84	12.26	309.51	0.96
$(100)4_{04}$-$(000)5_{33}$	3371.05	4.52	1.48	12.51	503.97	0.77
$(201)1_{01}$-$(200)2_{02}$	3367.19	4.17	1.20	13.91	67.77	0.81
$(200)3_{13}$-$(001)4_{14}$	3360.99	10.25	1.07	27.05	221.33	0.88
$(001)5_{32}$-$(000)6_{51}$	3359.52	3.43	1.54	3.28	888.63	0.47
$(201)1_{10}$-$(200)2_{11}$	3359.40			8.20	91.67	0.77
$(021)1_{10}$-$(030)2_{11}$	2142.37	44.67	17.49	1.03	110.41	0.92
$(100)5_{24}$-$(010)5_{15}$	2142.31			1.47	328.08	0.91
$(001)2_{21}$-$(010)2_{20}$	2142.26			64.75	148.74	0.96
$(001)2_{12}$-$(010)2_{11}$	2139.93	15.69	19.00	47.21	98.90	0.89
July/09/2008, ν_7-band of C_2H_6 at 79K – gfactors x 10^{-6} The line IDs indicates the main spectral features, and the reported g-factors also include						

efficiencies from underlying P and R branches in the spectral range of the Q-branches.

$^{R}Q_4$	3000.21	89.86	2.17	15.85	90.81	0.87
$^{R}Q_2$	2993.46	149.40	2.22	25.60	73.30	0.91
$^{R}Q_1$	2990.08	163.87	2.08	30.71	63.13	0.81
$^{R}Q_0$	2986.72	246.69	1.93	39.74	56.56	0.95
$^{P}Q_1$	2983.38	184.55	2.03	30.67	58.10	0.96
$^{P}Q_2$	2980.08	134.20	2.10	25.81	67.43	0.79
$^{P}Q_3$	2976.79	133.26	2.30	21.96	81.82	0.95

July/10/2008, ν_7-band of C_2H_6 at 78K – gfactors x 10^{-6}

$^{R}Q_4$	3000.21	96.49	2.42	15.85	91.04	0.89
$^{R}Q_2$	2993.46	156.49	1.72	25.67	72.40	0.93
$^{R}Q_1$	2990.08	169.79	1.68	30.86	62.41	0.85
$^{R}Q_0$	2986.72	255.74	1.82	40.12	56.15	0.96
$^{P}Q_1$	2983.38	187.36	1.47	30.85	57.32	0.97
$^{P}Q_2$	2980.08	150.63	1.75	25.91	66.57	0.83
$^{P}Q_3$	2976.79	125.78	1.40	21.67	79.67	0.96

July/09/2008, ν_1-band of HCN at 84K – gfactors x 10^{-6}

R4	3325.95	30.98	1.60	20.35	29.56	0.79
R2	3320.22	32.72	1.30	19.05	8.87	0.87
R1	3317.33	16.68	1.82	14.71	2.96	0.98
R0	3314.41	11.24	1.12	8.13	0.00	0.61
P2	3305.54	29.07	1.19	16.29	8.87	0.89
P3	3302.55	43.08	1.81	22.12	17.74	0.98
P4	3299.53	44.67	1.25	25.49	29.56	0.97
P5	3296.49	47.07	1.43	26.17	44.34	0.95
P6	3293.43	32.76	2.21	24.54	62.08	0.92
P7	3290.35	35.10	1.43	21.22	82.77	0.73
P8	3287.25	30.21	1.26	17.21	106.42	0.91
P9	3284.13	20.56	1.72	13.09	133.02	0.96

July/09/2008, ν_3-band of CH_3OH at 80K – gfactors x 10^{-6}

Q-branch	2844.28	182.38	5.00	13.23	93.02	0.98

July/10/2008, ν_3-band of CH_3OH at 80K – gfactors x 10^{-6}

Q-branch	2844.26	192.91	4.21	13.23	93.02	0.98

July/10/2008, ν_1-band of CO at 80K – gfactors x 10^{-6}

R3	2158.30	76.54	28.05	15.45	23.07	0.49
R2	2154.60	97.10	26.51	16.72	11.54	0.55
R1	2150.86	96.82	18.79	12.58	3.85	0.65
P2	2135.55	107.98	26.43	14.91	11.54	0.66
P3	2131.63	97.17	24.33	18.36	23.07	0.57

July/09/2008, ν_3-band of CH_4 at 80K – gfactors x 10^{-6}						
R2 (E-E)	3048.17	11.72	2.94	11.26	31.44	0.01
R2 (F1-F2)	3048.15			16.95	31.44	0.04
R1 (F2-F1)	3038.50	15.01	2.66	17.21	10.48	0.20
R0 (A2-A1)	3028.75	24.28	2.76	20.57	0.00	0.20
P2 (E-E)	2999.06	7.19	3.04	4.46	31.44	0.01
P2 (F1-F2)	2998.99			6.69	31.44	0.24
July/09/2008, C_2H_2 at 80K – gfactors x 10^{-6}						
ν_3-band R9e	3317.88	3.74	1.16	5.80	105.89	0.85
ν_3-band R4e	3306.48	5.54	1.13	5.07	23.53	0.95
$\nu_2+\nu_4+\nu_5$ band R9e	3304.97	7.21	1.02	6.55	105.89	0.98
ν_3-band R3e	3304.17	12.69	1.16	14.98	14.12	0.97
$\nu_2+\nu_4+\nu_5$ band R7e	3300.42	6.19	1.65	11.29	65.89	0.58
ν_3-band R1e	3299.52	10.14	1.25	9.92	2.35	0.95
$\nu_2+\nu_4+\nu_5$ band R5e	3295.84	20.52	1.25	15.51	35.30	0.96
$\nu_2+\nu_4+\nu_5$ band R3e	3291.23	11.16	1.99	16.05	14.12	0.63
ν_3-band P3e	3287.75	11.65	1.10	14.97	14.12	0.94
$\nu_2+\nu_4+\nu_5$ band R1e	3286.58	12.43	1.28	10.70	2.35	0.96
ν_3-band P5e	3282.99	8.12	2.15	18.89	35.30	0.36
July/09/2008, ν_1-band NH_3 at 80K – gfactors x 10^{-6} Corresponding g-factors from Kawakita & Mumma 2011 are 1.25, 0.63 and 1.91 x 10^{-6}.						
Ortho $s^qP(1,0)$	3317.21	5.84	1.47	1.02	19.89	0.88
Para $a^qP(2,1)$	3295.43	11.87	1.25	0.56	56.71	0.96
Ortho $a^qP(2,0)$	3295.38			1.52	60.41	0.96

(*) Fluorescence efficiencies (g-factors) for C_2H_6 were calculated following Villanueva et al. 2011a; for H_2O following Villanueva et al. 2011d; for CH_4, C_2H_2 and CO the General-Fluorescence Model (Villanueva et al. 2011a) and considering revised spectroscopic parameters from HITRAN (Gordon et al. 2011; Rothman et al. 2009); for CH_3OH following Villanueva et al. 2011b; and for the nitrogen compounds (NH_3 and HCN) following Villanueva et al. 2011c.

TABLE 3. ROTATIONAL TEMPERATURES, PRODUCTION RATES AND MIXING RATIOS

NIRSPEC Setting	Parent Volatile	T_{rot} [K][a]	Q [10^{26} s^{-1}][b]	Mixing Ratio w.r.t. H_2O [%][c]	Mixing ratio assuming enhanced polar abundances [%][d]
		July 9, 2008			
KL1, KL2	H_2O	80 ± 2	120.32 ± 8.90	100.00	100.00
	CH_4	(80)	1.89 ± 0.23	1.57 ± 0.16	0.63
KL1	CH_3OH	(80)	4.55 ± 0.35	3.78 ± 0.12	3.78
	C_2H_6	79 ± 3	2.37 ± 0.15	1.96 ± 0.04	0.78
KL2	H_2CO	(80)	< 0.14 (3σ)	< 0.12 (3σ)	< 0.05
	HCN	84 ± 5	0.61 ± 0.04	0.50 ± 0.01	0.20
	C_2H_2	(80)	0.34 ± 0.03	0.29 ± 0.02	0.12
	NH_3	(80)	2.09 ± 0.24	1.74 ± 0.17	0.70
		July 10, 2008			
KL1, MWA	H_2O	79 ± 3	122.34 ± 9.11	100.00	100.00
KL1	CH_3OH	(80)	4.84 ± 0.37	3.96 ± 0.12	3.96
	C_2H_6	78 ± 3	2.44 ± 0.15	1.99 ± 0.05	0.78
MWA	CO	(80)	5.52 ± 0.71	4.50 ± 0.51	1.8

a) Rotational temperatures with confidence limits are obtained from the analysis of multiple lines. Values in parenthesis are assumed.

b) The uncertainties (1σ) reflect the level of agreement among production rates obtained independently from different lines, and include uncertainties in compensation for slit-losses (q-scale). In addition we verified that the reported values are (at worst) only weakly influenced by the uncertainties in rotational temperature. Non-detections are defined at the 3σ stochastic level.

c) Mixing ratios relative to symmetric water (source I). The uncertainties reflect the level of agreement among production rates obtained independently from different lines of the corresponding volatile and H_2O. Q-scale uncertainties are not included since all instrument settings sample H_2O lines.

d) Considering the existence of an extended source of water, the mixing ratios for the apolar species are expected to be lower if all sources are included. It is very difficult to determine the strength of source II from our observations, but from the column densities reported in Table 4, we estimate the global water production (sources I and II) of the polar species to be at least 2.5 higher than what we measure for source I only (see section 3.1).

TABLE 4. WATER COLUMN DENSITIES ALONG THE SLIT

Pixel	**Distance** [km]	**Seeing loss**	**Water I** column x 10^{18} [molecules m^{-2}]	**Water II** column x 10^{18} [molecules m^{-2}]	**Excess ratio** II/(I+II) [%]
+4	200	1.17	14.5	0.0	0
+3	150	1.14	20.1	0.3	2
+2	100	0.95	32.8	0.2	1
+1	50	0.57	70.4	0.0	0
Center	0	0.26	168.9	5.0	3
-1	50	0.57	71.7	7.3	9
-2	100	0.95	35.1	10.9	24
-3	150	1.14	22.2	14.4	39
-4	200	1.17	17.5	14.6	46
-5	250	1.15	15.6	13.4	46
-6	300	1.10	11.9	15.6	57
-7	350	1.07	10.1	16.1	62
-8	400	1.04	9.2	16.0	63
-9	450	1.02	7.8	15.8	67
-10	500	1.02	6.1	14.7	71
-11	550	1.01	5.8	12.8	69
-12	600	1.01	6.6	10.0	60
-13	650	1.01	4.8	9.2	66
-14	700	1.01	3.7	11.5	76
-15	750	1.00	2.9	11.0	79
-16	800	1.00	2.0	11.5	85

The pixel number indicates the instrumental pixel along the slit of the measurement, and its position (+, -). Each pixel has a field of view of 0.432"x0.198" or 110 x 50 km^2. The spectral extracts used to retrieve the molecular abundances reported in Table 3 are marked in gray (central 9-rows) with a total FOV of 0.432"x 1.782" (110 x 450 km^2). Slit losses due to "atmospheric seeing" were computed using a seeing model with a point-spread-function (PSF) of 0.7" (full-width-half-maximum, FWHM). The reported molecular column densities for both water sources have been corrected for slit losses to assist in the extraction of production rates, and in the future development of outgassing models for source II.

TABLE 5. POSSIBLE COSMOGONIC INDICATORS

Molecule	Indicator	Value	Formation Temperature
Water (H_2O)	D/H	$< 12.9 \times 10^{-4}$ (3σ)	> 14 K[(a)]
	ortho/para ratio	2.87 ± 0.15 (1σ)	> 34 [(b)]
Methane (CH_4)	R0, R1, R2 and P2	F/A = 1.57 ± 0.48 (1σ) E/A < 11.31 (3σ)	> 19 K[(c)]

(a) The measured D/H corresponds to a formation temperature higher than 14K (3σ) assuming the model by Millar et al. 1989 for dense interstellar clouds that have reached thermal equilibrium and are dominated by gas-phase chemistry. Our HDO/H_2O upper limit (< 0.0026, 3σ) is significantly smaller than values predicted for the protoplanetary disk (~0.03 at disk mid-plane) in recent models (Willacy & Woods 2009). A D/H in water of 12.9×10^{-4} corresponds to 8.3 VSMOW.

(b) Considering the 1σ uncertainties, the OPR ranges from 2.72 to equilibrium, and corresponds to a spin temperature higher than 34 K.

(c) The upper-limit for methane spin temperature was derived from the 1σ uncertainty of the F/A range (1.09 to equilibrium), and corresponds to $T_{spin} > 19K$. The spin temperature implied by the 3σ upper-limit for the E/A ratio is consistent with this estimate.

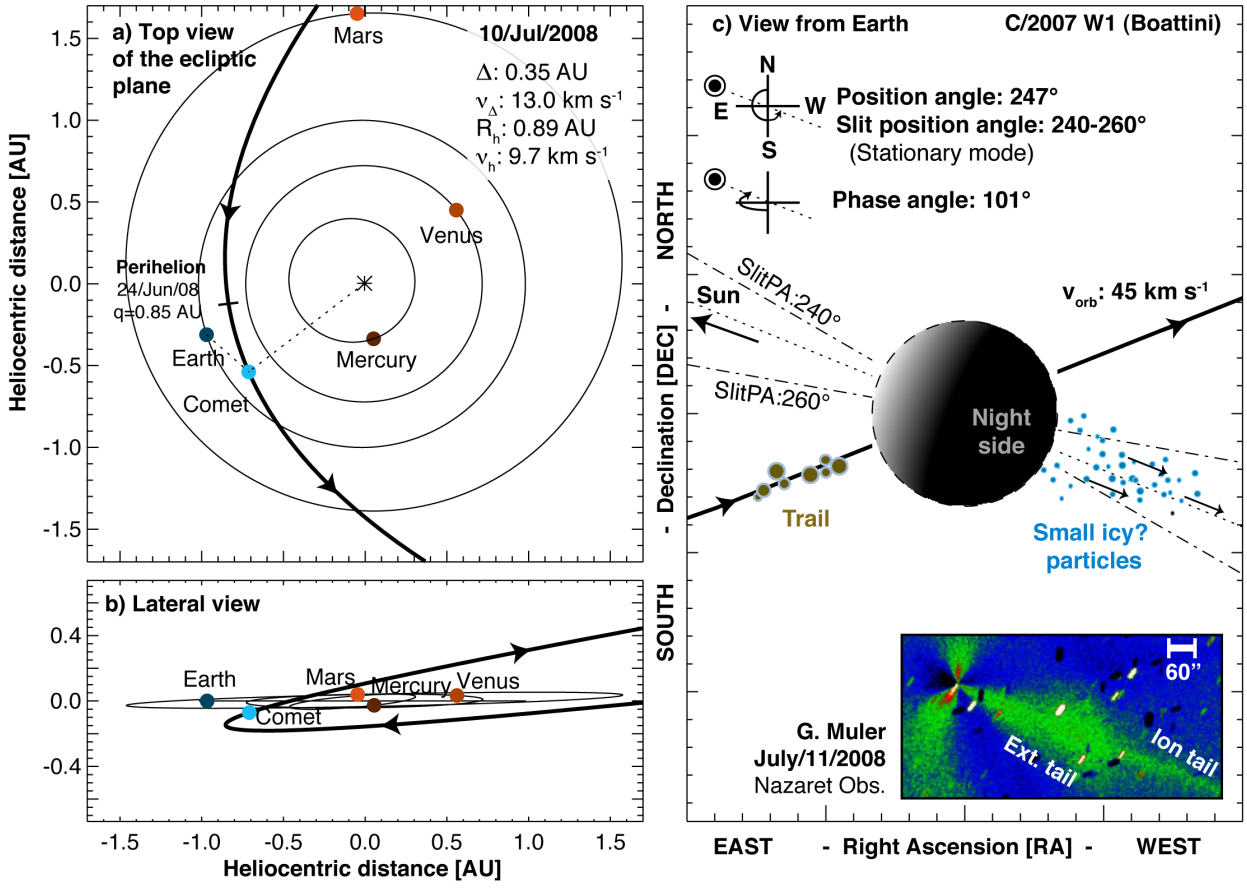

FIGURE 1: Diagrams showing the position and orbit of the comet (panels 'a' and 'b') during the observations in July 2008, with panel 'c' presenting the projection as observed from Earth. The observations were performed just after perihelion, and the instrument slit was oriented along the Sun-Comet radius vector projected onto the sky plane. In panel 'c' we include an image of comet Boattini taken by Gustavo Muler on July/11/2008 using the Nazaret Observatory (Lanzarote, Spain) with a clear optical filter, processed using the Larson-Sekanina numerical approach (rotational shift difference) to enhance anisotropic excesses. The image shows a narrow ion tail and an emission 'cloud' (distinct from the narrow ion tail) extended in the anti-sunward direction. Small icy particles are preferentially affected by solar pressure and solar actuated non-gravitational jet forces leading to a possible enhancement of these particles in the anti-sunward direction. Solar wind pickup of charged icy grains could also be at work beyond the ionopause.

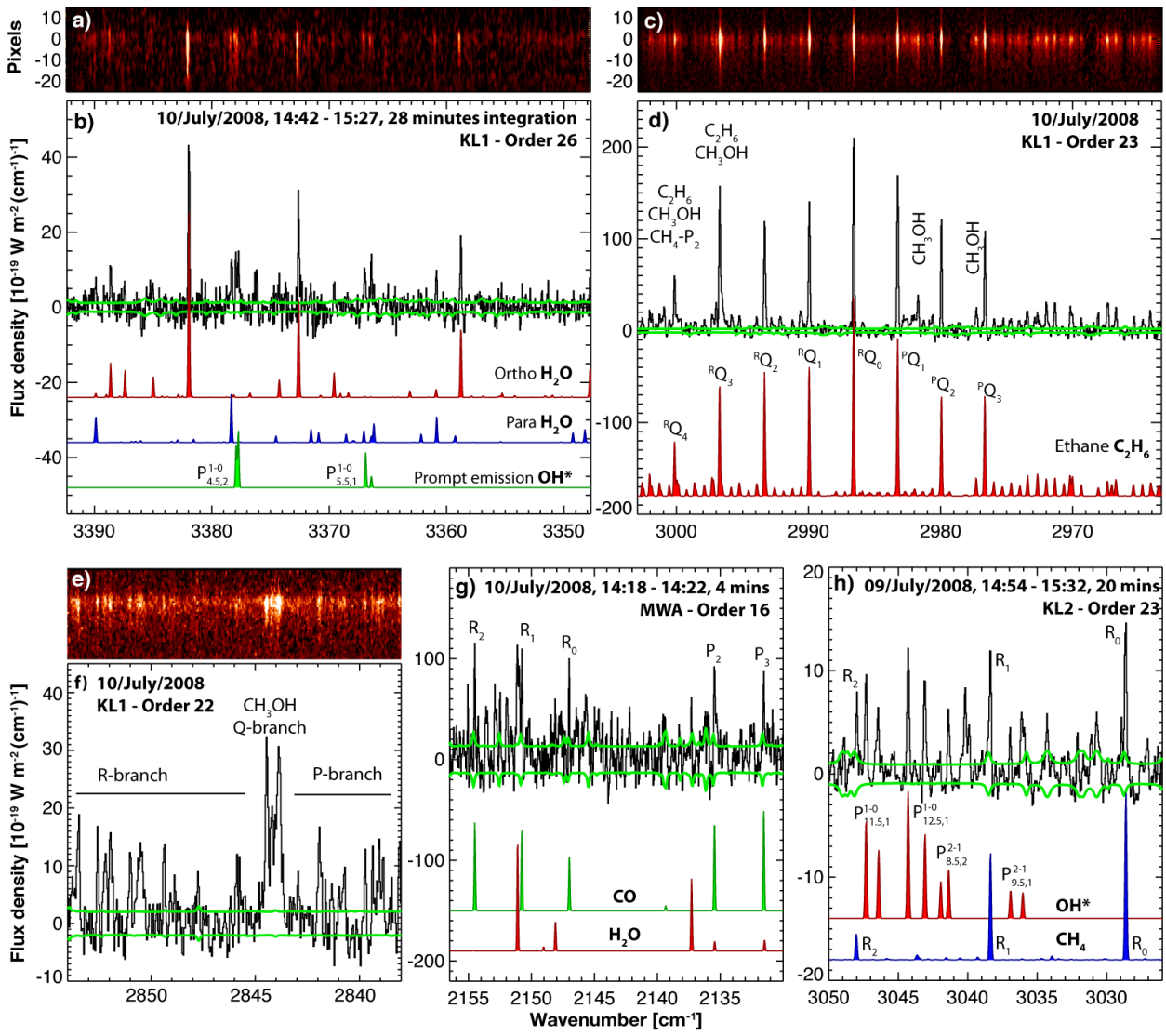

FIGURE 2: Detection of parent volatiles in comet C/2007 W1 (Boattini). Panels 'a' and 'c' show echellograms for KL1 (order 26) and KL1 (order 23) measured simultaneously with NIRSPEC (the cross-dispersed echelle spectrometer at Keck II) on UT 10 July 2008; the corresponding spectral extracts (± 4 rows from the nucleus) are presented in panels 'b' and 'd' showing bright emissions of H_2O, OH* (prompt-emission), C_2H_6 and CH_3OH. Detection of the Q-, P- and R-branches of the ν_3-band of CH_3OH are observed in panel 'e' and 'f', while panel 'g' shows the simultaneous detection of CO and H_2O at longer wavelengths using the MWA filter. Panel 'h' shows the detection of CH_4 and the best-fit fluorescence model assuming a rotational temperature of 80K. 1-sigma error levels are presented with light green traces.

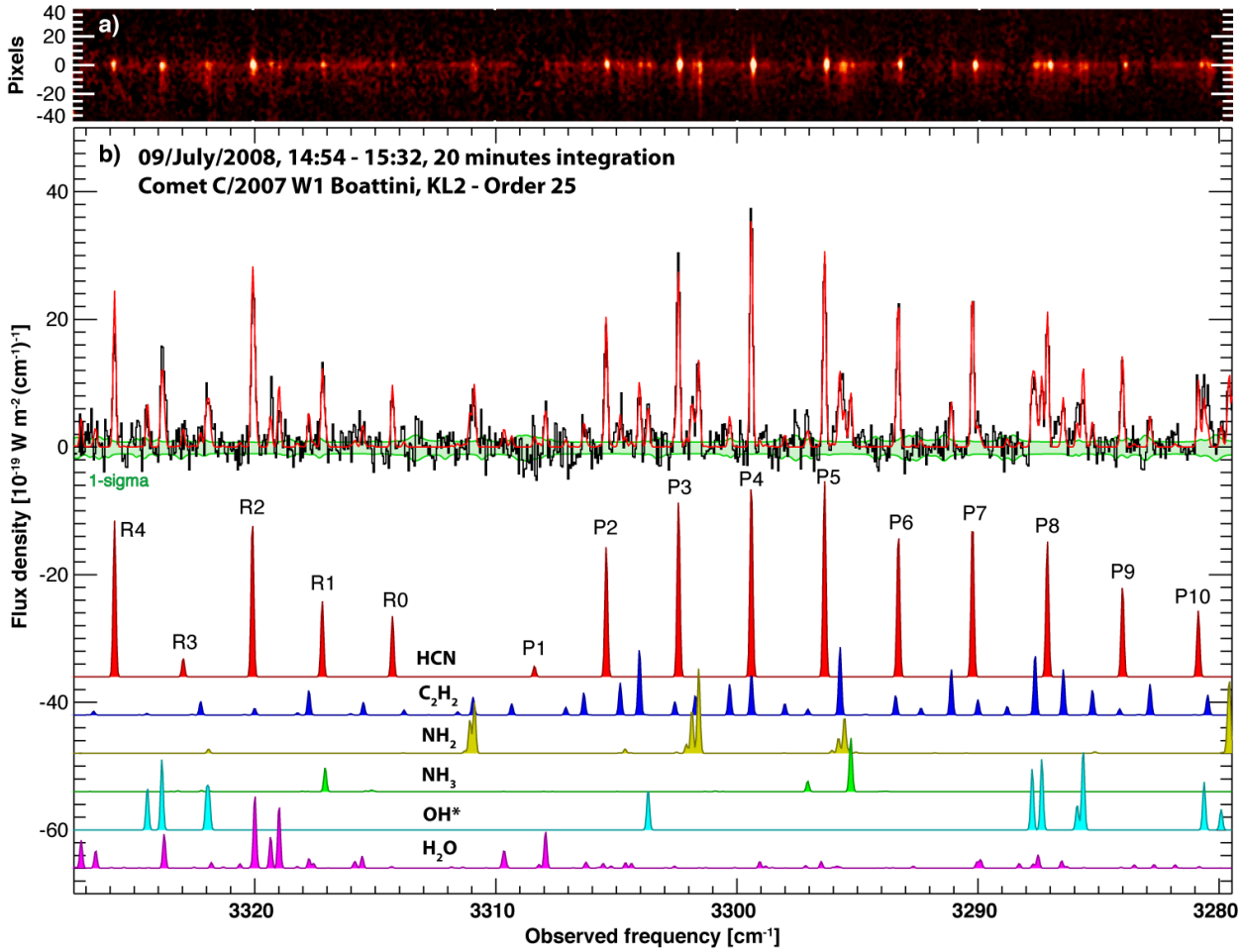

FIGURE 3: Echellogram and spectral extract obtained using the KL2 setting (order 25) on UT 9 July 2008. Panel 'a' shows emission of multiple parent volatiles and their evident spatial dichotomy. H_2O, OH* (prompt emission) and NH_2 lines show particularly asymmetric spatial profiles contrasting strongly with the bright and spatially symmetric HCN lines. Retrieval of line-by-line production rates were obtained from this rich spectrum by performing a "global" fit, in which all species were retrieved simultaneously, thereby properly accounting for spectral blends. See text for additional detail.

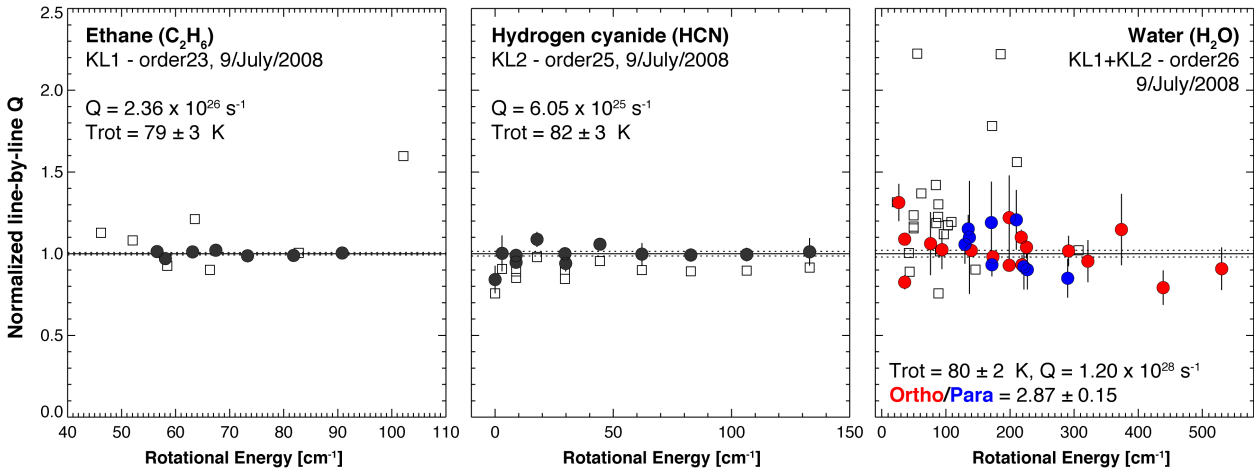

FIGURE 4: Excitation analysis of C_2H_6 (KL1 setting), HCN (KL2 setting) and H_2O (KL1 and KL2 settings). In this analysis, an optimum temperature produces a horizontal profile, in which production rates retrieved from lines with different excitation energy are consistent. The solid horizontal line at 1.0 indicates the normalizing Q, which is the weighted mean using the new model. Dotted lines present the ± 1σ standard error of the distribution. Individual error bars are presented with vertical lines. We retrieved independent rotational temperatures for the three species, and for the case of water we also retrieved the spin temperature from the ortho/para ratio. Production rates were obtained using the newly developed models for C_2H_6 (ν_7-band), HCN (ν_1-band) and H_2O (full non-resonance fluorescence); see text for details. Values considering the previous models (w.r.t. to the new models) are shown with square boxes.

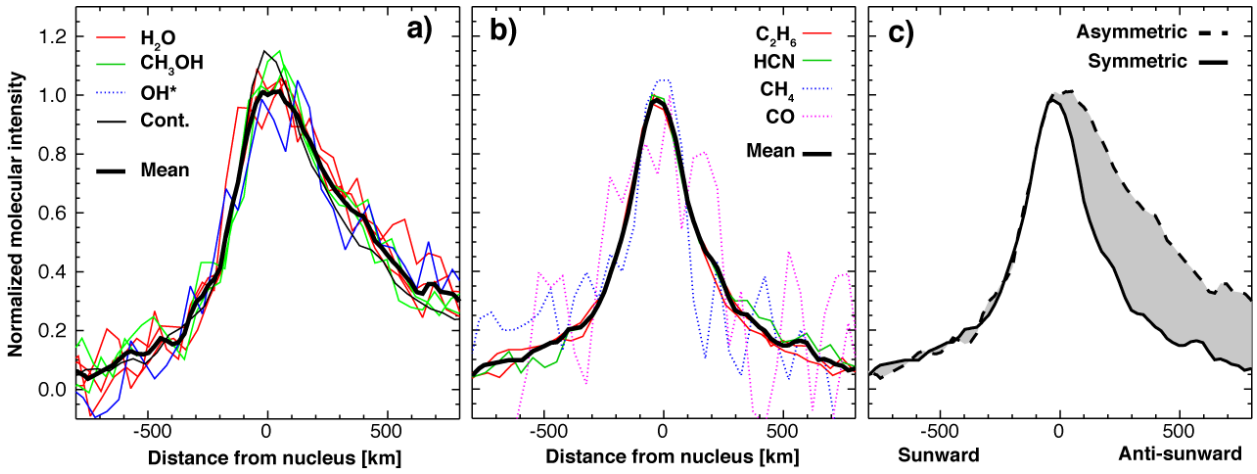

FIGURE 5: Spatial profile analysis for multiple species. Panel 'a' shows the spatial profiles of the polar molecules CH_3OH and H_2O, the product OH* (prompt emission), and the continuum intensity of KL1 order 23 (see figure 6 also). Panel 'b' shows the symmetric profiles of C_2H_6 and HCN, and the weakly resolved spatial profiles of CH_4 and CO. Panel 'c' shows a comparison of the two types of spatial profiles, which were computed by performing a weighted mean of the profiles presented in panels 'a' and 'b'. Extracted column densities are presented in Table 4.

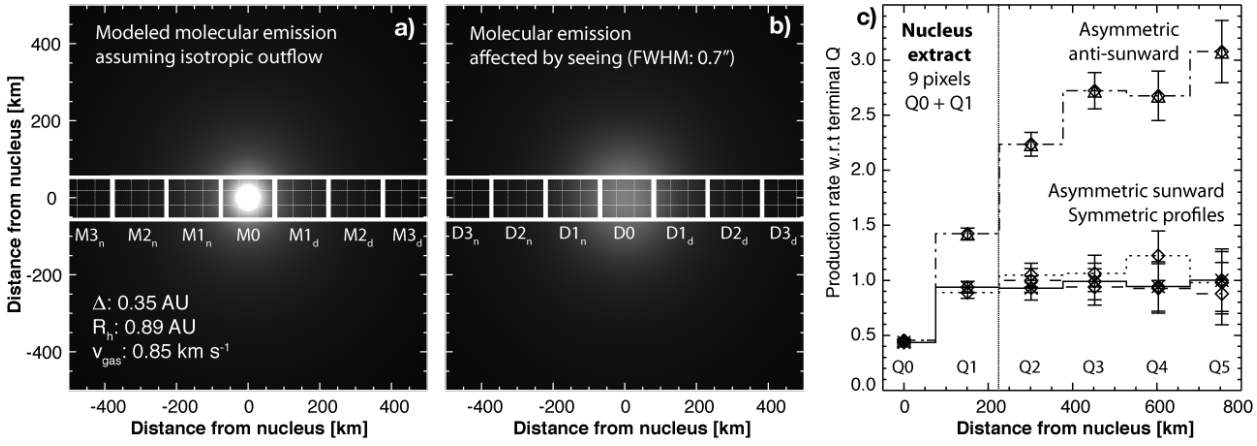

FIGURE 6: Modeling and retrieval of production rates. Panel 'a' shows a two-dimensional synthetic image of the expected emission of comet C/2007 W1 (Boattini) with isotropic outflow without seeing effects, where the horizontal grid shows the instrument pixelation (3x0.144" = 0.432" wide and 0.198"/pixel along the slit). The MX_y blocks indicate binning extracts for the ***model flux***, where X indicates distance along the slit from the nucleus and y is 'n' for night-side and 'd' for dayside. Panel 'b' reveals the effects of "seeing" in the observed data where DX_y shows the integration area of the ***observed fluxes***. Panel 'c' shows the D/M ratio between observed (DX_y) and modeled (MX_y) fluxes for the asymmetric and symmetric profiles. Spectral extracts presented in Figs. 2 and 3 were obtained from the central 9 pixels ($D1_n$ + D0 + $D1_d$), corresponding to an aperture of 0.432" x 1.782".

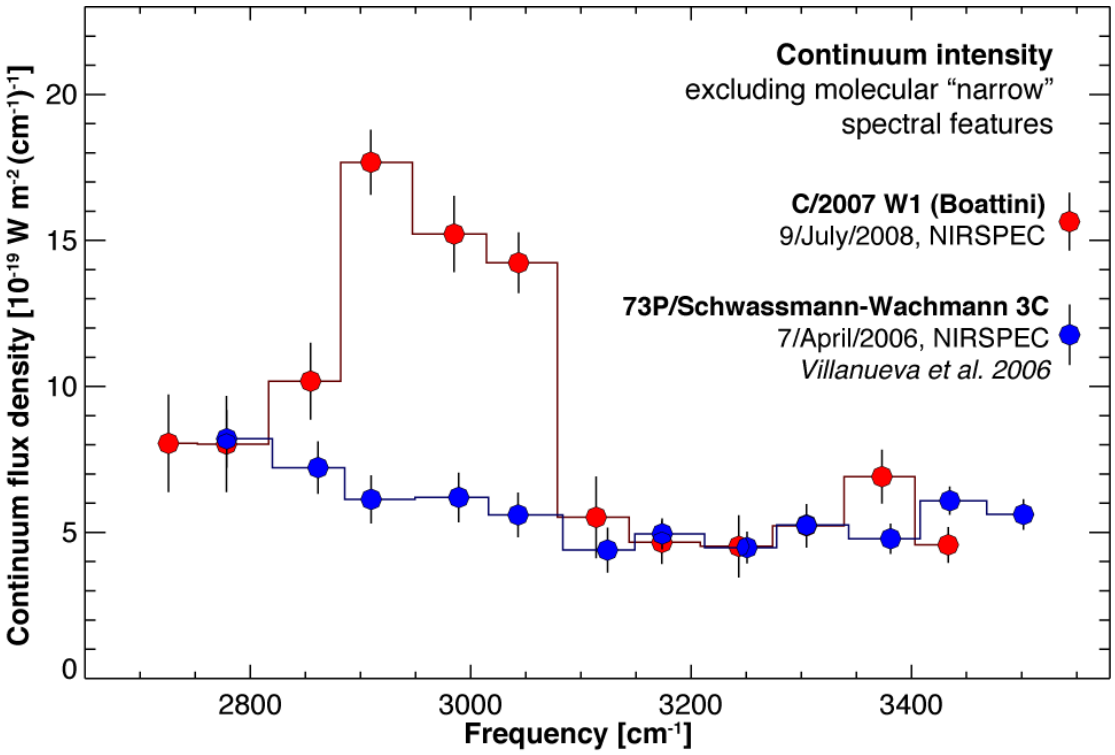

FIGURE 7: Continuum intensity of comet C/2007 W1 (Boattini) in comparison to comet 73P/Schwassmann-Wachmann 3C (Villanueva et al. 2006). The values for 73P were scaled by 0.7 to facilitate the comparison. We measured the continuum flux density at each order for both KL settings (12 measurements) while avoiding narrow spectral features. Comet Boattini presents abnormal excess intensity in the 2800-3100 cm^{-1} (3.6-3.2 μm) spectral range where many organic materials have strong emissions, peaking in order 23 of the KL1 setting. This excess could represent "organic refractory grains", "methanol-water ice grains", or the combined flux from several weak emission bands of ethane and methanol (plus other aliphatic and aromatic volatiles having bands in this spectral region).

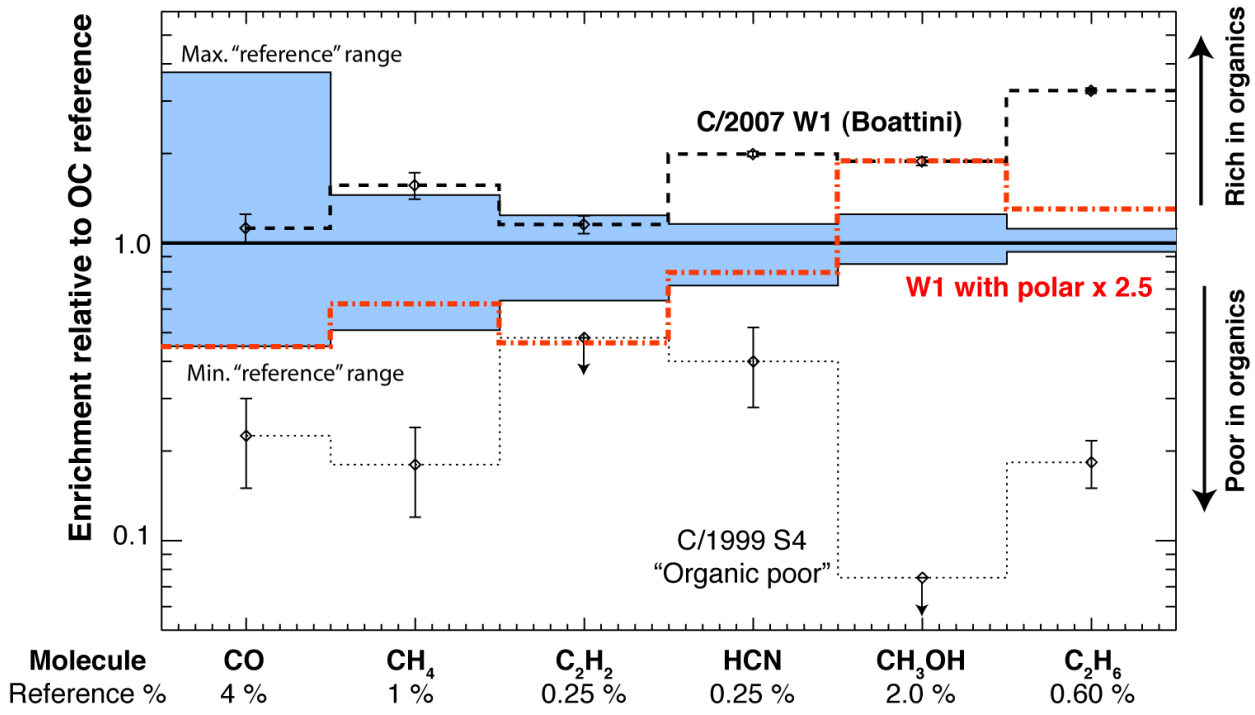

FIGURE 8: The composition of the Oort Cloud (OC) comet C/2007 W1 Boattini in comparison to other comets. The abundances are presented relative to a set of "reference" abundances of OC defined as unity. It is somewhat difficult to define a "reference" in abundances since comets show great diversity in their chemical taxonomies [e.g. Mumma et al. 2003, and refs. therein], and herewith we have defined as "reference" the median of values observed in other Oort-Cloud comets, heavily weighting the values of C/1996 B2 (Hyakutake), C/1995 O1 (Hale-Bopp) and C/1999 H1 (Lee) since these have been measured with high precision. In general, there is a relationship between the spread (blue zone) of the abundances among "normal" comets and the sublimation temperature, with the notable exception of C_2H_6. Comet C/1999 S4 (Mumma et al. 2001) is generally poor in organics, and Boattini shows enhancements in all volatiles (dotted line), and in particular for HCN, CH_3OH and C_2H_6 which are good indicators for chemical enrichment. The red dash-dotted line indicates the organic composition of comet Boattini if we assume a higher amount (by a factor of 2.5, see section 3.1) of polar species (H_2O, CH_3OH) in the inner coma than from source I only.

References

A'Hearn, M.F., Belton, M.J.S., Delamere, W.A., Kissel, J., Klaasen, K.P., McFadden, L.A., Meech, K.J., Melosh, H.J., Schultz, P.H., Sunshine, J.M., Thomas, P.C., Veverka, J., Yeomans, D.K., Baca, M.W., Busko, I.C., Crockett, C.J., Collins, S.M., Desnoyer, M., Eberhardy, C.A., Ernst, C.M., Farnham, T.L., Feaga, L.M., Groussin, O., Hampton, D.L., Ipatov, S.I., Li, J.-Y., Lindler, D.J., Lisse, C.M., Mastrodemos, N., Owen, T.C., Richardson, J.E., Wellnitz, D.D. & White, R.L. (2005). Deep Impact: Excavating Comet Tempel 1. *Science*. 310. p. 258.

A'Hearn, M.F., Belton, M.J.S., Delamere, W.A., Feaga, L.M., Hampton, D., Kissel, J., Klaasen, K.P., McFadden, L.A., Meech, K.J., Melosh, H.J., Schultz, P.H., Sunshine, J.M., Thomas, P.C., Veverka, J., Wellnitz, D.D., Yeomans, D.K., Besse, S., Bodewits, D., Bowling, T.J., Carcich, B.T., Collins, S.M., Farnham, T.L., Groussin, O., Hermalyn, B., Kelley, M.S., Kelley, M.S., Li, J.-Y., Lindler, D.J., Lisse, C.M., McLaughlin, S.A., Merlin, F., Protopapa, S., Richardson, J.E. & Williams, J.L. (2011). EPOXI at Comet Hartley 2. *Science*. 332 (6). pp. 1396–1400.

Barber, R.J., Tennyson, J., Harris, G.J. & Tolchenov, R.N. (2006). A high-accuracy computed water line list. *Monthly Notices of the Royal Astronomical Society*. 368. p. 1087.

Bonev, B.P. (2005). Towards a Chemical Taxonomy of Comets: Infrared Spectroscopic Methods for Quantitative Measurements of Cometary Water. *Ph.D. Thesis*. p. 322.

Bonev, B.P., Mumma, M.J., Villanueva, G.L., DiSanti, M.A., Ellis, R.S., Magee-Sauer, K. & Dello Russo, N. (2007). A Search for Variation in the H_2O Ortho-Para Ratio and Rotational Temperature in the Inner Coma of Comet C/2004 Q2 (Machholz). *The Astrophysical Journal*. 661 (1). pp. L97–L100.

Bonev, B.P., Mumma, M.J., Gibb, E.L., Di Santi, M.A., Villanueva, G.L., Magee-Sauer, K. & Ellis, R.S. (2009). Comet C/2004 Q2 (Machholz): Parent Volatiles, a Search for Deuterated Methane, and Constraint on the CH4 Spin Temperature. *The Astrophysical Journal*. 699 (2). pp. 1563–1572.

Bonev, B.P., Mumma, M.J., Kawakita, H., Kobayashi, H. & Villanueva, G.L. (2008). IRCS/Subaru observations of water in the inner coma of Comet 73P-B/Schwassmann Wachmann 3: Spatially resolved rotational temperatures and ortho para ratios. *Icarus*. 196 (1). pp. 241–248.

Dello Russo, N., DiSanti, M.A., Mumma, M.J., Magee-Sauer, K. & Rettig, T.W. (1998). Carbonyl Sulfide in Comets C/1996 B2 (Hyakutake) and C/1995 O1 (Hale-Bopp): Evidence for an Extended Source in Hale-Bopp. *Icarus*. 135 (2). pp. 377–388.

Dello Russo, N., Vervack, R.J., Weaver, H.A., Biver, N., Bockelée-Morvan, D., Crovisier, J. & Lisse, C.M. (2007). Compositional homogeneity in the fragmented comet 73P/Schwassmann-Wachmann 3. *Nature*. 448. p. 172.

Dello Russo, N., Mumma, M.J., DiSanti, M.A., Magee-Sauer, K. & Novak, R. (2001). Ethane Production and Release in Comet C/1995 O1 Hale-Bopp. *Icarus*. 153 (1). pp. 162–179.

Dello Russo, N., Vervack, R.J., Weaver, H.A., Montgomery, M.M., Deshpande, R., Fernández, Y.R. & Martin, E.L. (2008). The Volatile Composition of Comet 17P/Holmes after its Extraordinary Outburst. *The Astrophysical Journal*. 680. p. 793.

Dello Russo, N., Bonev, B.P., DiSanti, M.A., Mumma, M.J., Gibb, E.L., Magee-Sauer, K., Barber, R.J. & Tennyson, J. (2005). Water Production Rates, Rotational Temperatures, and Spin Temperatures in Comets C/1999 H1 (Lee), C/1999 S4, and C/2001 A2. *The Astrophysical Journal*. 621 (1). pp. 537–544.

DiSanti, M.A., Mumma, M.J., Dello Russo, N. & Magee-Sauer, K. (2001). Carbon Monoxide Production and Excitation in Comet C/1995 O1 (Hale-Bopp): Isolation of Native and Distributed CO Sources. *Icarus*. 153 (2). pp. 361–390.

DiSanti, M.A., Anderson, W.M., Villanueva, G.L., Bonev, B.P., Magee-Sauer, K., Gibb, E.L. & Mumma, M.J. (2007a). Depleted Carbon Monoxide in Fragment C of the Jupiter-Family Comet 73P/Schwassmann-Wachmann 3. *The Astrophysical Journal*. 661 (1). pp. L101–L104.

DiSanti, M.A., Bonev, B.P., Magee-Sauer, K., Russo, Dello, N., Mumma, M.J., Reuter, D.C. & Villanueva, G.L. (2006). Detection of Formaldehyde Emission in Comet C/2002 T7 (LINEAR) at Infrared Wavelengths: Line-by-Line Validation of Modeled Fluorescent Intensities. *The Astrophysical Journal*. 650 (1). pp. 470–483.

DiSanti, M.A., Villanueva, G.L., Bonev, B.P., Magee-Sauer, K., Lyke, J.E. & Mumma, M.J. (2007b). Temporal evolution of parent volatiles and dust in Comet 9P/Tempel 1 resulting from the Deep Impact experiment. *Icarus*. 187 (1). pp. 240–252.

Drouart, A., Dubrulle, B., Gautier, D. & Robert, F. (1999). Structure and Transport in the Solar Nebula from Constraints on Deuterium Enrichment and Giant Planets Formation. *Icarus*. 140. p. 129.

Gibb, E.L., Mumma, M.J., Russo, Dello, N., DiSanti, M.A. & Magee-Sauer, K. (2003). Methane in Oort cloud comets. *Icarus*. 165 (2). pp. 391–406.

Gordon, I., Villanueva, G.L., Jacquemart, D., Gomez, L., Nakawaga, K., Jolly, A. & Rothman, L. (2011). HITRAN Update for C_2H_2 (Acetylene). *HITRAN*. http://www.cfa.harvard.edu/hitran/updates.html#Acetylene%20update.

Harris, G.J., Tennyson, J., Kaminsky, B.M., Pavlenko, Y.V. & Jones, H.R.A. (2006). Improved HCN/HNC linelist, model atmospheres and synthetic spectra for WZ Cas. *Monthly Notices of the Royal Astronomical Society*. 367. p. 400.

Hiraoka, K., Takayama, T., Euchi, A., Handa, H. & Sato, T. (2000). Study of the Reactions of H and D Atoms with Solid C_2H_2, C_2H_4, and C_2H_6 at Cryogenic Temperatures. *The Astrophysical Journal*. 532 (2). pp. 1029–1037.

Horanyi, M. & Mendis, D.A. (1985). Trajectories of charged dust grains in the cometary environment. *The Astrophysical Journal*. 294. pp. 357–368.

Hudson, R.L. & Moore, M.H. (1999). Laboratory Studies of the Formation of Methanol and Other Organic Molecules by Water+Carbon Monoxide Radiolysis: Relevance to Comets, Icy Satellites, and Interstellar Ices. *Icarus*. 140 (2). pp. 451–461.

Jacquinet-Husson, N., Crépeau, L., Capelle, V., Scott, N.A., Armante, R. & Chédin, A. (2009). The GEISA Spectroscopic Database System in its latest Edition. *EGU General Assembly 2009*. 11. p. 1128.

Kawakita, H. & Mumma, M.J. (2011). Fluorescence Excitation Models of Ammonia and Amidogen Radical (NH_2) in Comets: Application to Comet C/2004 Q2 (Machholz). *The Astrophysical Journal*. 727 (2). p. 91.

Kawakita, H., Dello Russo, N., Furusho, R., Fuse, T., Watanabe, J.-I., Boice, D.C., Sadakane, K., Arimoto, N., Ohkubo, M. & Ohnishi, T. (2006). Ortho-to-Para Ratios of Water and Ammonia in Comet C/2001 Q4 (NEAT): Comparison of Nuclear Spin Temperatures of Water, Ammonia, and Methane. *The Astrophysical Journal*. 643. p. 1337.

Magee-Sauer, K., Mumma, M.J., DiSanti, M.A., Dello Russo, N., Gibb, E.L., Bonev, B.P. & Villanueva, G.L. (2008). The organic composition of Comet C/2001 A2 (LINEAR). I. Evidence for an unusual organic chemistry. *Icarus*. 194 (1). pp. 347–356.

Mandell, A.M., Mumma, M.J., Blake, G.A., Bonev, B.P., Villanueva, G.L. & Salyk, C. (2008). Discovery of OH in circumstellar Disks around Young Intermediate-Mass Stars. *The Astrophysical Journal*. 681. pp. L25–L28.

McLean, I.S., Becklin, E.E., Bendiksen, O., Brims, G., Canfield, J., Figer, D.F., Graham, J.R., Hare, J., Lacayanga, F., Larkin, J.E., Larson, S.B., Levenson, N., Magnone, N., Teplitz, H. & Wong, W. (1998). Design and development of NIRSPEC: a near-infrared echelle spectrograph for the Keck II telescope. *Proceedings of the Society of Photo-Optical Instrumentation Engineers (SPIE)*. 3354. p. 566.

Meech, K.J., et al. (2011). EPOXI: Comet 103P/Hartley 2 Observations from a Worldwide Campaign. *The Astrophysical Journal Letters*. 734 (1). p. L1.

Millar, T.J., Bennett, A. & Herbst, E. (1989). Deuterium fractionation in dense interstellar clouds. *The Astrophysical Journal*. 340. p. 906.

Morbidelli, A., Levison, H.F., Tsiganis, K. & Gomes, R. (2005). Chaotic capture of Jupiter's Trojan asteroids in the early Solar System. *Nature*. 435. p. 462.

Mousis, O., Gautier, D., Bockelée-Morvan, D., Robert, F., Dubrulle, B. & Drouart, A. (2000). Constraints on the Formation of Comets from D/H Ratios Measured in H_2O and HCN. *Icarus*. 148. p. 513.

Mumma, M.J. & Charnley, S.B. (2011). The Chemical Composition of Comets – Emerging

Taxonomies & Natal Heritage. *Annual Review of Astronomy and Astrophysics*. 49. pp. 471–524.

Mumma, M.J., DiSanti, M.A., Dello Russo, N., Fomenkova, M., Magee-Sauer, K., Kaminski, C.D. & Xie, D.X. (1996). Detection of Abundant Ethane and Methane, Along with Carbon Monoxide and Water, in Comet C/1996 B2 Hyakutake: Evidence for Interstellar Origin. *Science*. 272 (5). pp. 1310–1314.

Mumma, M.J., Russo, Dello, N., DiSanti, M.A., Magee-Sauer, K., Novak, R.E., Brittain, S., Rettig, T., McLean, I.S., Reuter, D.C. & Xu, L.-H. (2001). Organic Composition of C/1999 S4 (LINEAR): A Comet Formed Near Jupiter? *Science*. 292 (5). pp. 1334–1339.

Mumma, M.J., DiSanti, M.A., Magee-Sauer, K., Bonev, B.P., Villanueva, G.L., Kawakita, H., Dello Russo, N., Gibb, E.L., Blake, G.A., Lyke, J.E., Campbell, R.D., Aycock, J., Conrad, A. & Hill, G.M. (2005). Parent Volatiles in Comet 9P/Tempel 1: Before and After Impact. *Science*. 310 (5). pp. 270–274.

Mumma, M.J., DiSanti, M.A., Russo, Dello, N., Magee-Sauer, K., Gibb, E. & Novak, R. (2003). Remote infrared observations of parent volatiles in comets: A window on the early solar system. *Advances in Space Research*. 31 (1). pp. 2563–2575.

Mumma, M.J., Boncho, B.P., Villanueva, G.L., Paganini, L., Disanti, M.A., Gibb, E.L., Keane, J.V., Meech, K.J., Blake, G.A., Ellis, R.S., Lippi, M., Boehnhardt, H. & Magee-Sauer, K. (2011). Temporal and Spatial Aspects of Gas Release During the 2010 Apparition of Comet 103P/Hartley 2. *The Astrophysical Journal Letters*. 734 (L7). p. 6.

Mumma, M.J., Weaver, H.A. & Larson, H.P. (1987). The Ortho-Para Ratio of Water Vapor in Comet p/ Halley. *Astronomy and Astrophysics*. 187. p. 419.

Nakano, S. (2008). Comet C/2007 (Boattini) orbital computation. *Oriental Astronomical Association, http://www.oaa.gr.jp/~oaacs/nk.htm*.

Rothman, L.S., Gordon, I.E., Barber, R.J., Dothe, H., Gamache, R.R., Goldman, A., Perevalov, V.I., Tashkun, S.A. & Tennyson, J. (2010). HITEMP, the high-temperature molecular spectroscopic database. *Journal of Quantitative Spectroscopy and Radiative Transfer*. 111. p. 2139.

Rothman, L.S., et al. (2009). The HITRAN 2008 molecular spectroscopic database. *Journal of Quantitative Spectroscopy and Radiative Transfer*. 110. pp. 533–572.

Sunshine, J.M., A'Hearn, M.F., Groussin, O., Li, J.-Y., Belton, M.J.S., Delamere, W.A., Kissel, J., Klaasen, K.P., McFadden, L.A., Meech, K.J., Melosh, H.J., Schultz, P.H., Thomas, P.C., Veverka, J., Yeomans, D.K., Busko, I.C., Desnoyer, M., Farnham, T.L., Feaga, L.M., Hampton, D.L., Lindler, D.J., Lisse, C.M. & Wellnitz, D.D. (2006). Exposed Water Ice Deposits on the Surface of Comet 9P/Tempel 1. *Science*. 311. p. 1453.

Tozzi, G.P., Lara, L.M., Kolokolova, L., Boehnhardt, H., Licandro, J. & Schulz, R. (2004). Sublimating components in the coma of comet C/2000 WM1 (LINEAR). *Astronomy and*

Astrophysics. 424. p. 325.

Villanueva, G.L., Mumma, M.J., Bonev, B.P., Di Santi, M.A., Gibb, E.L., Böhnhardt, H. & Lippi, M. (2009). A Sensitive Search for Deuterated Water in Comet 8P/Tuttle. *The Astrophysical Journal Letters*. 690 (1). pp. L5–L9.

Villanueva, G.L., Mumma, M.J., Novak, R.E. & Hewagama, T. (2008). Discovery of multiple bands of isotopic CO_2 in the prime spectral regions used when searching for CH_4 and HDO on Mars. *Journal of Quantitative Spectroscopy and Radiative Transfer*. 109. pp. 883–894.

Villanueva, G.L., Mumma, M.J. & Magee-Sauer, K. (2011a). Ethane in planetary and cometary atmospheres: Transmittance and fluorescence models of the ν_7 band at 3.3 μm. *Journal of Geophysical Research - Planets*. In press, http://astrobiology.gsfc.nasa.gov/Villanueva/papers/2011_ethane.pdf.

Villanueva, G.L., DiSanti, M.A. & Mumma, M.J. (2011b). Methanol (CH_3OH) in Planetary and Cometary Atmospheres. *The Astrophysical Journal*. In preparation.

Villanueva, G.L., Magee-Sauer, K. & Mumma, M.J. (2011c). Nitrogen compounds in Planetary and Cometary Atmospheres: Transmittance and Fluorescence models of Ammonia (NH_3) and Hydrogen-Cyanide (HCN). *Journal of Quantitative Spectroscopy and Radiative Transfer*. In preparation.

Villanueva, G.L., Bonev, B.P., Mumma, M.J., Magee-Sauer, K., DiSanti, M.A., Salyk, C. & Blake, G.A. (2006). The Volatile Composition of the Split Ecliptic comet 73P/Schwassmann-Wachmann 3: A Comparison of Fragments C and B. *The Astrophysical Journal*. 650 (1). pp. L87–L90.

Villanueva, G.L., Mumma, M.J., Bonev, B.P., Novak, R.E., Barber, R.J. & DiSanti, M.A. (2011d). Water in Planetary and Cometary Amospheres: H_2O and HDO Transmittances and Fluorescence Models. *Journal of Quantitative Spectroscopy and Radiative Transfer*. Submitted.

Watanabe, N., Nagaoka, A., Shiraki, T. & Kouchi, A. (2004). Hydrogenation of CO on Pure Solid CO and CO-H2O Mixed Ice. *The Astrophysical Journal*. 616. p. 638.

Willacy, K. & Woods, P.M. (2009). Deuterium Chemistry in Protoplanetary Disks. II. The Inner 30 AU. *The Astrophysical Journal*. 703. p. 479.

Xie, X. & Mumma, M.J. (1996). Monte Carlo Simulation of Cometary Atmospheres: Application to Comet P/Halley at the Time of the Giotto Spacecraft Encounter. II. Axisymmetric Model. *The Astrophysical Journal*. 464. p. 457.

Yurchenko, S.N., Barber, R.J. & Tennyson, J. (2011). A variationally computed line list for hot NH_3. *Monthly Notices of the Royal Astronomical Society*. 413 (3). pp. 1828–1834.

Yurchenko, S.N., Barber, R.J., Yachmenev, A., Thiel, W., Jensen, P. & Tennyson, J. (2009). A

Variationally Computed T = 300 K Line List for NH_3. *The Journal of Physical Chemistry A*. 113. p. 11845.